Benthic phosphorus cycling in the Peruvian Oxygen Minimum Zone

U. Lomnitz[1], S. Sommer[1], A. W. Dale[1], C. R. Löscher[1], A. Noffke[2], K. Wallmann[1] and C. Hensen[1]

[1]{GEOMAR Helmholtz Centre for Ocean Research Kiel, Wischhofstr. 1–3, 24148 Kiel, Germany}

[2]{Institut für Seenforschung (ISF) der LUBW, Argenweg 50/1, 88085 Langenargen, Germany}

Correspondence to: U. Lomnitz (ulomnitz@geomar.de)

Abstract

Oxygen minimum zones (OMZs) that impinge on continental margins favor the release of phosphorus (P) from the sediments to the water column, enhancing primary productivity and the maintenance or expansion of low-oxygen waters. A comprehensive field program in the Peruvian OMZ was undertaken to identify the sources of benthic P at six stations, including the analysis of particles from the water column, surface sediments and pore fluids as well as in situ benthic flux measurements. A major fraction of solid phase P was bound as particulate inorganic P (PIP) both in the water column and in sediments. Sedimentary PIP increased with depth in the sediment at the expense of particulate organic P (POP). The ratio of particulate organic carbon (POC) to POP exceeded the Redfield ratio both in the water column (202 ± 29) and in surface sediments (303 ± 77). However, the POC to total particulate P (TPP = POP + PIP) ratio was close to Redfield in the water column (103 ± 9) and in sediment samples (102 ± 15 This suggests that the relative burial efficiencies of POC and TPP are similar under low oxygen conditions and that the sediments underlying the anoxic waters on the Peru margin are not depleted in P compared to Redfield. Benthic fluxes of dissolved P were extremely high (up to 1.04 ± 0.31 mmol m^{-2} d^{-1}), however, showing that a lack of oxygen promotes the intensified release of dissolved P from sediments, whilst preserving the POC/TPP burial ratio. Benthic dissolved P fluxes were always higher than the TPP rain rate to the seabed, which is proposed to be caused by transient P release by bacterial mats that had stored P during previous periods when bottom waters were less reducing. At one station located at the lower rim of the OMZ, dissolved P was taken up by the sediments indicating ongoing phosphorite formation. This is further supported by decreasing porewater phosphate concentrations with sediment depth, whereas solid phase P concentrations were comparatively high. At this site, the POC/TPP and POC/PIP ratios dropped from average water-column values (close to Redfield for POC/TPP and POC/PIP ~250) to very low sedimentary ratios of ~ 7 (POC/TPP and POC/PIP), indicative of intensive P enrichment in the sediments.

1 Introduction

Phosphorus is an essential nutrient; it serves as an energy carrier for all living species and is a limiting macronutrient for marine primary production on geological time scales [Ingall and Jahnke, 1994; Föllmi, 1996; McManus et al., 1997; Filippelli, 2002; Paytan and McLaughlin,

2007; Tsandev et al., 2012; Ruttenberg, 2014]. Due to its impact on marine primary production, the oceanic phosphorus inventory modulates the atmospheric CO_2 level and Earth's climate [Ganeshram et al., 2002; Wallmann, 2003; Ingall, 2010]. Hence, it is crucial to understand feedback mechanisms of the P cycle to make future predictions.

Particulate and dissolved phosphorus in the ocean originate from terrestrial chemical weathering of the P containing mineral group of apatite [Filippelli, 2002]. Only around 30% of the P discharged to the oceans is potentially bioavailable [Compton et al., 2000] as dissolved P, inorganic P adsorbed minerals or associated with metal oxides and P bound within particulate organic matter. However, the largest fraction of the fluvial P is trapped in estuaries or buried in continental margin sediments and thereby removed from the P cycle before it reaches the open ocean [Compton et al., 2000]. The delivery of P to the sediments in the open ocean is mainly composed of organic and inorganic P associated with the export of organic detritus and other particles from the photic zone. P adsorbed to minerals such as Mn and Fe (oxyhydr)oxides [Föllmi, 1996; Delany, 1998; Faul et al., 2005] are further sources, as well as P input from fish debris that could be particularly important in productive upwelling regions [Suess, 1981; Schenau and DeLange, 2001; Dìaz-Ochoa et al., 2009; Noffke, 2014].

P cycling is strongly affected by redox-dependent processes. P can be scavenged by Fe (oxyhydr)oxides in oxic sediment and released across the sediment-water interface due to the reduction dissolution of Fe (oxyhydr)oxides in anoxic sediments [Sundby et al., 1986; Slomp et al., 1998]. Furthermore, recent studies showed that sulfur bacteria found in surface sediments of anoxic environments can internally store and release P under oscillating redox conditions [Ingall and Jahnke, 1997 and references therein]. Therefore, these organisms are a key player for the modulation of porewater P concentrations and benthic P release to the water column.

Additionally, hypoxic or anoxic conditions favor the precipitation of P in the form of authigenic carbonate fluorapatie (CFA) [Froelich et al., 1988; Suess and von Huene, 1988; Goldhammer et al., 2010; Ingall, 2010; Schenau and De Lange, 2000]. For non-upwelling areas, the required phosphate oversaturation in the porewaters has been attributed to the reductive dissolution of P bearing Fe (oxyhydr)oxides [e.g. Ruttenberg and Berner, 1993, Slomp et al., 1996]. In contrast, the CFA formation in sediments of the Namibian upwelling area was linked to microbial P release into the porewaters [Schulz and Schulz, 2005].

The resulting feedback on oceanic primary production and atmospheric O_2 and CO_2 levels triggered by changes in benthic P sequestration is still unclear. Presently, three opposing have been raised: (1) Intensified phosphate release from the sediments to the water column caused by an expansion of low oxygen waters [Ingall and Jahnke, 1994; Stramma et al., 2008] could stimulate the primary production in the surface waters [Wallmann, 2003]. This, in turn, may lead to a more intensified oxygen demand and a positive feedback with benthic P release [Slomp and Van Cappellen, 2007; Wallmann, 2010; Moffit et al., 2015]. (2) A negative feedback on P release has been postulated based on observations of CFA mineral precipitation found in the present-day oxygen depleted upwelling areas [Schulz and Schulz, 2005; Arning et al., 2009a; Arning et al., 2009b; Goldhammer et al., 2010; Cosmidis et al., 2013]. Being a major sink for bioavailable P [Delaney, 1998; Ingall, 2010], it has been argued that the expansion of OMZs may increase the CFA precipitation in the sediments and thus mitigate the benthic phosphate release [Ganeshram et al., 2002; Goldhammer et al., 2010; Ingall, 2010]. (3) A third scenario suggests that the formation of CFA is in balance with enhanced P release from anoxic sediments, implying that the dissolved oceanic P inventory is largely unaffected by oxygen concentrations [Delaney, 1998; Anderson et al., 2001; Roth et al., 2014]. These conflicting scenarios show that there is further need to explore the benthic-pelagic P cycling in oxygen deficient environments in order to enable improved predictions.

In this study, we explore P cycling in the Peruvian OMZ to identify and quantify P sources to the sediment and the return of inorganic dissolved P back to the water column. Our data set comprises samples of particulate matter from the water column as well as porewater, sediment samples and samples of filamentous sulfur bacteria. We present in situ benthic phosphate fluxes, particulate matter C/P ratios for water-column particles and surface sediments and P burial fluxes, and relative abundances of sulfur bacteria for 6 stations along the depth transect across the Peruvian shelf at 12°S. From a mass balance for P cycling in the sediments, we conclude that the benthic P sources and sinks were, in general, imbalanced during our sampling campaign.

2 Study Area

The study area is located in the center of the Peruvian OMZ at 12°S covering the shallow shelf from ~70 m water depth to mid-slope depths of about at ~400 m (Fig. 1). During our

106 sampling campaign in January 2013 neutral or slightly negative El Niño-Southern Oscillation
107 (ENSO) conditions dominated (http://www.cpc.ncep.noaa.gov) and the bottom water oxygen
108 concentrations were below detection limit of the Winkler titration (5 µmol L^{-1}) down to ~ 450
109 m water depth (Fig. 1, Table 1). Below the OMZ, oxygen concentrations increased to 19 and
110 53µM at 770 m and 1025 m water depth, respectively. Nitrate concentrations were below 12
111 µM from 128 to 407 m water depth (Table 1). During the measuring period, the bottom water
112 at station I (74 m) was sulfidic and depleted in nitrate (Table 1; Sommer et al., in review).

113 The oxygen deficient waters off Peru belong to one of the world's most prominent OMZ.
114 Southeasterly trade winds that are driven by the Pacific Subtropical Anticyclone engender
115 offshore transport of surface waters and upwelling of subsurface waters from the poleward
116 propagating Peru undercurrent (PUC) [Strub et al., 1998]. These water masses are oxygen
117 depleted and rich in nutrients, favoring primary production of up to 3.6 g C m^{-2} d^{-1} in surface
118 waters [Pennington et al., 2006]. As a consequence, the intense oxygen consumption induced
119 by the degradation of sinking particulate organic matter and a sluggish ventilation induce the
120 development of a strong OMZ. Based on the definition that the oxycline of an OMZ is at ~22
121 µM [Fuenzalida et al., 2009], the Peruvian OMZ extends from approximately 50 – 700 m
122 water depth. The greatest upwelling strength is reached during austral winter and spring
123 between 5 and 15°S [Strub et al., 1998]. The phases of strong upwelling are followed by high
124 rates of primary production in austral summer. The coastal area off Peru displays a highly
125 variable hydrographic regime. Especially during positive ENSO periods coastal trapped
126 waves emerging from equatorial Kelvin waves in the equatorial East Pacific occur frequently
127 [Gutiérrez et al., 2008 and references therein; Mosch et al., 2012]. Consequently, the
128 thermocline and the oxycline shift downwards by ca. 100 m and bottom-water oxygen
129 concentrations can increase from practically zero to around 100 µM in days to weeks
130 [Gutiérrez et al., 2008; Schunck et al., 2013; Graco et al., 2016]. Seasonally, bottom waters of
131 the shelf (75 m) can transition from oxic or hypoxic between austral winter/spring (low
132 primary production) to anoxic throughout the rest of the year [Noffke et al., 2012].
133 Furthermore, porewater uranium (U) profiles at 11°S indicate variable redox conditions at the
134 upper rim of the OMZ [Scholz et al., 2011]. The shelf area above 200m water depth is
135 therefore characterized by non-steady state conditions, whereas the oxygen concentrations in
136 the core OMZ (~200-400 m water depth) are predominantly below detection limit throughout
137 the year.

The sediments of the Peruvian OMZ have POC contents ranging from 15-20 wt. % within the OMZ and > 5 wt. % below the OMZ and on the shelf[Dale et al., 2015]. The fine-grained, diatomaceous mud lens between 11°S and 15°S accumulates under low PUC bottom-water velocities in 50 to 500 m water depth [Krissek et al., 1980]. This favors high sedimentation rates, carbon preservation and burial [Suess et al., 1987; Dale et al., 2015]. Further down, at mid-slope depth, a high energy regime favoring erosive settings leads to the formation of phosphorites [Reimers and Suess, 1983; Glenn and Arthur, 1988; Arning et al., 2009b; Mosch et al., 2012]. Another interesting observation between 70 and ~ 300 m of water depth is the occurrence of mat-forming filamentous sulfur bacteria [Mosch et al., 2012]. Bacterial mats are not conspicuous below below 300 to 400 m water depth, and instead foraminiferal sands are more common.

3 Methods

Sampling of water-column particulate matter and sediment cores as well as the deployment of the benthic landers BIGO I and II (Biogeochemical Observatories) were conducted along the 12°S depth transect during the RV *Meteor* cruise M92 in January 2013. The geographical position and water-column properties for the main stations are reported in Table 1. The data set on in situ phosphate fluxes comprised 10 stations from 74 to 989 m water depth. The wat

ercolumn particle sampling was performed at 6 stations from 74 to 407 m water depth. These stations are considered as main stations and for consistency the stations are numbered according to the data set published in Dale et al. (2015). Hydrographic parameters and oxygen concentrations were obtained by deploying a CTD/rosette equipped with a Seabird oxygen sensor (detection limit is 5 µM) calibrated by Winkler titration.

3.1 Water-column particles

Particulate matter was filtered using water from Niskin bottles from the CTD/rosette and analyzed for total particulate phosphorus (TPP), particulate inorganic phosphorus (PIP) and particulate organic carbon (POC) concentrations. Following Labry et al. (2013), we expect the PIP phase to be comprised of inorganic P phases originating from abiotic particulate P as well as inorganic P from biogenic particulate P. Abiotic PIP comprises detrital P associated to

minerals from terrigenous sources. Biotic PIP is composed of orthophosphates, pyrophosphates and polyphosphates within eukaryotic and prokaryotic cells.

Between three and six water depths were sampled per station. The water was filled into 10 L PE containers rinsed beforehand with ultrapure water (MilliQ). The containers were shaken before filtration which was performed within 24 h after sample retrieval. Approximately 2 to 4 L of seawater were filtered through pre-weighed and combusted (450°C, 5h) 0.7 µM Whatman GF/F filter using a seawater vacuum pump and Duran bottle top filters. After filtration, all filters were immediately frozen at -20°C. At the shore-based laboratory the GF/F filters were dried over night at 45°C, and divided into 3 equally sized pieces using a scalpel. The total filtered water volume was divided by three to calculate elemental concentrations on each filter section assuming homogenous coverage of particles on the filters.

3.1.1 Total particulate phosphorus (TPP), particulate inorganic phosphorus (PIP) and particulate organic phosphorus (POP)

The determination of TPP and PIP concentrations by combustion and colorimetric methods has been described by Asahi et al. (2014), Aspila et al. (1976), Loh and Bauer (2000) and others. However, the combustion and acid dissolution (HTC/hydrolysis) that has been applied for PIP-determination is limited by the fact that polyphosphates are only partly hydrolysed, but provides the best compromise compared to other methods (Labry et al., 2013). Although polyphosphates are underestimated, it includes intracellular P that is often dominant in plankton and only small amounts of organic P. In the case of TPP we used the Aspila (1976) method without an oxidant (e.g. $MgSO_4$) during combustion, which underestimates the TPP concentration in water-column particles. However, for the sediments, the results following of the Aspila (1976) method were compared total digestions showing an average recovery of the Aspila method of approximately 102%. In two samples we found an overestimation in total digestion of more than 100% and in one sample an underestimation of 32%, possibly due to heterogeneity of the samples caused by very small phosphorite granules.

Filter segments for TPP concentration were combusted at 550°C for 90 min and afterwards soaked with 20 ml 1 N hydrochloric acid (HCl) and shaken for 24 h at room temperature. Then, the solution was filtered and 0.35 ml triple reagent (40 ml 9.8 N sulfuric acid, 12 ml ammonium molybdate and 4 ml potassium antimonyl tartrate solution) and 0.175 ml ascorbic acid and 3 ml 1 N HCl were added to 3.75 ml of the sample solution. Then, 0.3 ml of 12.5 N

198 sodium hydroxide (NaOH) was added to the solution before colorimetric measurement of
199 phosphate at 880 nm using a Hitachi U-2001 photospectrometer. This was done because test
200 runs with the standard series revealed that the slope of the calibration curve was not steep
201 enough to measure the low phosphate concentrations expected. To resolve this issue, the pH
202 of the solution was slightly increased usingg NaOH. Measurements were accompanied using
203 a standard series consisting of 8 standards ranging from 5 to 100 µM PO_4^{3-}, prepared from a
204 Merck phosphate stock solution. We used 0.75 ml of each standard for the standard series and
205 treated each of them in the same manner as described above. The samples were measured
206 undiluted due to low concentrations and the technical detection limit of a 1 cm cuvette.
207 Hence, we used 3.75 ml of the filtered sample solution, added the reagents mentioned above
208 and divided the concentrations by a factor of 5 to adjust the results to those of the standard
209 series. A factor of 0.02 was used to transform the concentration unit to µmol L^{-1}. The amount
210 of filtered water (f) refers to 1/3 of the total filtered water volume (f is different for each
211 sample):

$$\text{TPP or PIP } [\mu\text{mol L}^{-1}] = \frac{[PO_4^{3-}] \cdot 0.02}{5 \cdot f}$$ The same procedure was

212 ### 3.1.2 Organic carbon concentration

213 The filter sections for the analysis of POC concentration were fumed with 37 % HCl
214 overnight to remove inorganic carbon, dried and wrapped into tin caps. Samples were
215 measured by flash combustion with a Carlo Erba elemental analyzer (NA1500). The
216 analytical precision and detection limit were 0.04 dry wt. %.The water-column POC
217 concentrations are given in µmol L^{-1}.

218 ## 3.2 Porewater and solid phase analysis

219 Sediment cores were recovered using video-guided multiple corers (MUC) equipped with
220 PVC liners with an inner diameter of 10 cm. The porewater and solid phase sub-sampling was
221 performed immediately after recovery in an argon-filled glove bag at in situ seafloor
222 temperature. The bottom water was siphoned with a plastic tube and filtered through cellulose
223 acetate filters. Afterwards, the cores were sectioned into 0.5 cm intervals from 0-5 cm
224 sediment depth and 1 cm intervals afterwards. The sediment samples were filled into
225 centrifuge tubes and the porewater was separated from the sediments by centrifuging for 20

min at ~ 3940 G (centrifuge force). The supernatant porewater was filtered through cellulose acetate filters inside the glove bag. Samples were immediately analyzed for total dissolved phosphate (TPO_4) and dissolved ferrous iron (Fe^{2+}) after pore water extraction using a Hitachi U-2001 spectrophotometer. The analyses were performed according to the standard techniques described in Grasshoff et al. (1999). A sediment subsample was taken from each sediment depth and stored refrigerated in pre-weighed air-tight plastic cups to determine the water content, porosity and total organic carbon (TOC) content. The residual sediments were stored frozen at -20°C (sediment and filter samples) and the pore water samples were refrigerated at 4°C for land-based analytics.

The TOC concentration (in μmol mg^{-1}) of freeze-dried and ground sediment samples was determined by flash combustion in a Carlo Erba Elemental Analyzer (NA 1500). For POC determination, samples were decalcified with 2.5 N HCl prior to the measurement. Solid phase TPP and PIP concentrations were measured according to the method of Aspila et al. (1976) in a similar manner as described before for the water-column particles. 50 mg of freeze-dried and ground sediment were digested in 1N HCl for a minimum of 24 hours to dissolve the sedimentary PIP phase. Sediment portions analyzed for TPP were combusted at 550°C for 90 min before adding 1 N HCl. The solutions were filtered and the reagents mentioned above were added prior to measurement. We used the sedimentary reference standards SDO-1 (Devonian Ohio Shale, USGS; Govindaraju, 1994) and MESS-3 (Marine Sediment Reference Material, Canadian Research Council) and replicate measurements of samples to ensure measurement accuracy. The standard series applied to the measurements covered a concentration range from 5 to 100 μM.

To determine the terrigenous P input to the sediments, and to calculate the TPP burial flux (for calculation see section 3.6 and Table 2), sediments were analyzed using total digestion. About 100 mg of freeze dried and ground sediment was digested in hydrofluoric acid (40%, supra pure), nitric acid (65%, supra pure) and perchloric acid (60%, supra pure). For measurement accuracy the reference standards SDO-1 and MESS-3 as well as methodological blanks were included in the analysis. The aluminum concentration in the digestion solutions was measured using an inductively coupled plasma optical emission spectrometer (ICP-OES, Varian 720 ES). The relative standard deviation (RSD) for [Al] was found to be < 1%.

The XRD data of core 107MUC23 from 407 m water depth were obtained from approximately 1 g of freeze dried and ground sediment in the lab of the University of Bremen.

3.3 POC in relation to various fractions of P (POC/xP ratios)

The molar POC/xP ratios (where xP = TPP, PIP or POP) of the water column particles at stations I, IV and V were calculated from measurements on two filter samples per water depth. For these samples a minimum and maximum value was calculated. For the other stations III, VI and VIII, only one sample per water depth was available. Here, we assumed an average nutral variability calculated from the duplicate measurements of stations I, IV and V for each P species (supplementary material). For sediment samples we calculated a standard deviation for each station (supplementary material). For sediment samples we calculated a standard deviation from repeated measurements of the sediment standards MESS-3 and SDO-1 (supplementary material).

3.4 Benthic lander fluxes

Benthic lander deployments were performed at 10 stations along the 12°S transect (I to X according to Dale et al., 2015). In situ benthic fluxes were obtained using the two BIGOs I and II (BIGO: Biogeochemical Observatory). They were equipped with two circular flux chambers (internal diameter 28.8 cm, area 651.4 cm^2) [Sommer et al., 2009]. An online video-controlled launch system allowed precise placement of the BIGO at the seafloor directly located beneath the particle sampling stations in the water column and in proximity to the multi-corer stations. After a 4 hour rest period at the seafloor during which surrounding bottom water was periodically flushed into the chamber, the chambers were slowly driven into the sediment. The BIGOs stayed for 28 hours at the seafloor, while 8 water samples per chamber were taken via glass syringes. In order to obtain bottom water background information, additional samples were taken every 8 hours from the ambient bottom water. Phosphate concentrations in the syringe samples were measured on board using an auto analyzer. The standard series covered a concentration range from 0.05 to 3.5 µM. The fluxes were calculated from the slope of linear regression of all 8 data points versus the sampling time (supplementary material) and corrected for the water volume in the chamber and the dead volume of the 1 m long Vygon tubes connecting the syringes with the flux chambers. The error caused by the dilution from the dead volume of these tubes was calculated from the

chloride concentration measured in the syringe samples. Benthic lander TPO_4 fluxes for most sites are based on two replicate chamber measurements. The uncertainty given for the TPO_4 fluxes is the difference between the minimum and maximum fluxes from the average of the two benthic chambers. At two stations (IV and V), it was only possible to calculate the flux from one chamber. For further details on the benthic flux measurements during the M92 cruise see Dale et al. (2015).

3.5 Diffusive flux calculations

The diffusive fluxes of TPO_4 and Fe^{2+} from the sediment to the bottom water were calculated by applying Fick's First Law of diffusion:

$$F_{TPO4/Fe2+} = - \phi D_{SED} (\mathrm{d}[C]/\mathrm{d}x) \qquad (1)$$

where the term $\mathrm{d}[C]/\mathrm{d}x$ describes the concentration gradient between the bottom water and the first porewater sample of the surface sediment divided by the corresponding sediment depth (0.25 cm or 0.5 cm) and ϕ is the porosity of the surface sediment. The diffusion coefficient, D_{SED}, for sediments was calculated according:

$$D_{SED} = D_{SW}/\theta^2 \qquad (2)$$

The diffusion coefficients for TPO_4 and Fe^{2+} under standard conditions (D_{SW}) under standard conditions (298.15 K and 1 bar) were taken from Li and Gregory (1974) and corrected for the in situ temperature and pressure using the Stokes-Einstein equation. The tortuosity (θ^2) was derived from the sediments porosity according to the modified Weissberg formulation [Boudreau,1996]:

$$\theta^2 = 1 - \ln(\phi^2) \qquad (3)$$

Uncertainty in the diffusive flux was calculated at St. I as the difference between the fluxes calculated from two separate sediment cores. For the other stations, only one core was available to calculate the flux.

3.6 Mass balance of benthic phosphorus cycling

To investigate benthic P cycling quantitatively, a mass balance was developed considering P input, P burial, and P release. The equations for the P mass balance calculations are shown in

Table 2. Under steady state conditions, the total P rain rate should balance the P buried in the sediments and the benthic TPO_4 flux (Eq. 4 in Table 2). The rain rates of particulate P delivered to the sediments are differentiated in inorganic P (RR_{PIP}) (Eq. 5 in Table 2) and organic P (RR_{POP}) (Eq. 6, Table 2). The rates were calculated using the POC/xP ratio of the water column particles that were taken as close as possible to the seafloor at each station (2-5 m above ground) and the POC rain rate (RR_{POC}) (Table 4 and supplementary material). RR_{POC} for the same stations along the 12°S transect were previously calculated by Dale et al. (2015) as the sum of the measured benthic DIC flux and the POC accumulation rate. The terrigenous P input (RR_{Pterr}) (Eq. 7 in Table 2) can be estimated by multiplying the solid phase Al concentration of the first sediment sample by the mass accumulation rate [Dale et al., 2015] and a P/Al ratio of 0.02 that characterizes the P/Al ratio of riverine particles originating from the continent [Viers et al., 2009].

The P burial flux (F_{Pbur}) (Eq. 8 in Table 2) was calculated by multiplying the mass accumulation rate (MAR) and the average solid phase P concentration of the first 11 sediment centimeters (P_{11}) (11 cm is due to our sampling resolution). This approach was chosen according to Dale et al. (2015) who also calculated POC accumulation rate for the OMZ stations (i.e. not on the shelf or below the OMZ) using the elemental average concentration of the first 10 cm of sediment. MAR (Eq. 9 in Table 2) was calculated from the sedimentation rate (ω_{acc} in cm y^{-1}), dry bulk density (ρ_{dry}; in g cm^{-3}) and the average porosity of the sediments at the lower core end (ϕ_{∞}). Sedimentation accumulation rates were determined from particle-bound $^{210}Pb_{xs}$ measurements using a modeling approach. A detailed method description and the values used for this work are published in Dale et al. (2015). The error derived from modeling the sedimentation rate was given as 20 % and propagates to all subsequent calculations where it was used.

3.7 Freeze/thaw experiments

In order to determine the amount of polyphosphate stored in sulfide-oxidizing bacteria, foraminifera and other bacteria we conducted additional sediment experiments at all transect stations, except station IV. Sediments from MUC corers were sliced into 1 cm thick slices from the surface sediment to 10 cm sediment depth. Before phosphate analysis, sediment slices were repeatedly frozen at -80°C and defrosted in order to burst microbial cells and release the internally stored P to the porewater.

3.8 Molecular quantification of filamentous bacteria

In order to quantify the abundance of filamentous microbes at the benthic boundary layer, we used a molecular approach. Nucleic acid purification was performed on 0.5 g sediment following established protocols [Bertics et al., 2013]. DNA was quality checked on an agarose gel and quantified using a Nanodrop spectrophotometer (Peqlab, Erlangen, Germany). 16S rDNA fragments were taken from a previously generated metagenome from this region (GenBank Bioproject PRJNA280940) and the respective sequence counting's were deposited at GenBank (ID KU312264-KU312267). Sequencing was carried out in the Institute of Clinical Molecular Biology at Kiel University. Sequences were analyzed using a Clustal W alignment tool on Mega 6 [Tamura et al., 2013]. A qPCR primer and probe set was established using the Primer Express software (Life Technologies, Carlsbad, USA) with the forward primer 5' AGAAGCACCGGCTAACTCTG-3' , the reverse primer,

5' -CCAGGTAAGGTTCTTCGCGT-3' and the probe 829-Thioploca 5'-GGATTAATTTCCCCCAACAT-3' [Teske et al., 1995]. Primers and probes were tested *in silico* on the Silva database and cross amplification was excluded on a variety of 16S rDNA clones. The qPCRs were performed in technical duplicates on a ViiA7 system (Life Technologies, Carlsbad, USA) as previously described [Löscher et al., 2012] using 1x TaqMan PCR buffer (Life Technologies, Carlsbad, USA), 2.5 pmol μL^{-1} TaqMan probe, 5 pmol μl^{-1} of each primer, 400 ng μl^{-1} bovine serum albumin (to avoid PCR inhibition without affecting standard curves or detection limits), 3 µl PCR water, and 5 µl of either standard DNA or environmental sample. A plasmid containing the target sequence was used to generate a standard dilution series for absolute quantification. The melting temperature was set to 50°C. A theoretical detection limit of 4 copies per PCR reaction was calculated. The results of the analysis are given in copies g^{-1} of 16S rDNA sequences of sulfur bacteria that are related to Marithioploca.

4 Results

4.1 P composition of water-column particulate matter and surface sediments

4.1.1 TPP, PIP, POP and POC concentrations

The TPP concentrations ranged from 0.02 to 0.2 μmol L^{-1} in the water-column particles and from 0.04 to 2.37 μmol mg^{-1} in the surface sediments (supplementary material). Overall, the profiles along the transect show no significant trends through the water column (Fig. 2A). The highest concentrations occurred in the surface waters around 10 m of water depth. At stations I, V and VIII (74, 195 and 407 m) the TPP concentrations slightly increased close to the seafloor, whereas at the other stations no such trend was observed (Fig. 2A and supplementary material). In the sediments the TPP concentrations slightly decreased with sediment depth, except at station VIII (407 m). Here, the highest sedimentary TPP concentrations across the transect were found at 2.25 cm sediment depth (17 μmol mg^{-1}). Below that depth the concentrations decreased, but remained high compared to the other stations.

The PIP and POP concentrations (water column and sediments) generally followed the trends of the TPP profiles and contributed roughly equally to TPP. The PIP fraction accounted for 21 to 74 % of TPP in the water-column particles (Fig. 3), similar as reported in previous studies [Paytan et al., 2003; Faul et al., 2005; Benitez-Nelson et al., 2007; Lyons et al., 2011; Sekula-Wood et al., 2012]. At stations I, VI and VIII (74, 244 and 407 m), the PIP concentrations were larger than POP. The opposite occurred at station V (195 m) where the POP fraction was clearly larger than the PIP fraction throughout the entire water column. In comparison to the water-column particles, the PIP fraction was larger than POP in most samples reaching between 48 to 98% of TPP. However, the strongest deviation between PIP and POP concentrations was found in the sediments of station VIII (407 m) where the PIP concentration was up to a factor of ~ 50 larger than the POP concentration and comprised up to 98% of TPP. XRD data from that station revealed that 7 to 16 wt.% of the sediments consisted of apatite and other P-bearing minerals (data not shown).

The particulate organic carbon concentrations ranged from 2.2 to 17.6 μmol L^{-1} in the water-column particles and from 2.8 to 13.4 μmol mg^{-1} in the surface sediments. Within the water column the highest concentrations occurred in the surface water samples, while the

concentration measured at station VI (244 m) is about 5 times higher than compared to other samples from the same water depth. Below the surface water concentration peak, the concentrations were on average 7 μmol L^{-1} with distinct depth trends. The sedimentary POC concentrations were on average 7.7 μmol mg^{-1} for the whole transect. Overall, the POC concentrations showed little variability with sediment depth. At station III, VI and VIII (128, 244 and 407 m) the concentrations increased slightly with sediment depth. At station I (74 m) the concentration decreased slightly with sediment depth.

4.2 Particulate organic carbon to phosphorus (POP, PIP, TPP) ratios

POC/POP ratios

The molar POC/POP ratios of the water-column particles and of the surface sediments were consistently higher than the Redfield ratio at all stations (Fig. 2B). The average POC/POP ratio of the water-column particles was 202 ± 29. There was no clear trend through the water column, except slightly increasing ratios between the deepest water-column samples and the surface sediment samples. In the surface sediments, the ratios increased within the upper 6 cm with an average POC/POP ratio of 303 ± 77. Station VIII (407 m) is an exception, and here the ratio decreased to 81 within the first ~ 2 cm of sediment and then strongly increased to ≥600.

POC/PIP ratios

The average POC/PIP ratio of the water-column particles was 248 ± 34. Similar to the POC/POP ratios, there was no significant trend through the water column. At the majority of the stations, the ratios decreased close to the seabed. The average POC/PIP ratio of the surface sediments was 184 ± 34 and almost invariable with water depth. In the sediments, the ratios showed no significant down-core trend. At station VIII (407 m) the ratio in the sediments showed a dramatic decrease compared to the water column, with an average of 7, similar to the POC/TPP ratios (below).

POC/TPP ratios

The POC/TPP ratios of the water-column particles and surface sediments consistently varied around the Redfield ratio. The exceptions are station I (74 m) and the deepest station (Sta. VIII, 407 m). At station I, the sediments showed significantly lower than Redfield ratios with

an average of 69 in the surface sediments. The average POC/TPP ratio of the surface sediments at station VIII (407 m) was 7. Between the deepest water-column sample and the first sediment sample, the POC/TPP ratios were rather constant without a consistent trend, again with the exception of station VIII (407 m) where the ratios decreased sharply.

4.3 In situ benthic chamber fluxes

The benthic lander TPO_4 fluxes (F_{TPO4}) are presented in Table 3 and Fig. 4A. Positive fluxes are defined as directed from the sediments into the water column. The highest TPO_4 flux along the depth transect of 1.04 ± 0.31 mmol m^{-2} d^{-1} occurred at station I (74 m). Below 74 m water depth, fluxes decreased by at least a factor of 3 to 0.2 – 0.3 mmol m^2 d^{-1} at 144 m water depth. Measurements at station V (195 m) showed a slightly increased TPO_4 flux of 0.44 ± 0.07 mmol m^{-2} d^{-1}, while the fluxes measured at 244 m (St. VI) and 306 m (St. VII) decreased to the before mentioned levels. At 407 m water depth (St. VIII) the TPO_4 flux was negative, indicating a phosphate uptake by the sediment. Below the OMZ, the fluxes increased to slightly positive values, but remained low at 0.06 and 0.02 ± 0.02 mmol m^{-2} d^{-1}.

4.3.1 Comparison of benthic chamber TPO_4 fluxes and diffusive TPO_4 fluxes

The measured benthic chamber TPO_4 fluxes and the calculated diffusive TPO_4 fluxes showed large discrepancies. The calculated diffusive fluxes were consistently higher than the benthic fluxes (Table 4, Fig. 4B). In contrast to the in situ measured benthic chamber TPO_4 release rates, the calculation of diffusive TPO_4 fluxes relies on bottom water and pore water PO_4^{3-} concentrations. A subsurface PO_4^{3-} peak occurred at all stations in the uppermost depth interval at 0-0.25 cm causing a large concentration gradient between the bottom water and the pore water PO_4^{3-} concentrations (Fig. 7). Even though the measured benthic TPO_4 fluxes exceeded the fluxes that could be generated by TPP degradation by a factor of approximately 6, the diffusive TPO_4 fluxes were still higher (Table 4). Hence, the diffusive TPO_4 flux will be referred to as potential TPO_4 flux in the following.

4.4 TPP burial fluxes and TPP burial efficiency

The P burial fluxes decreased with increasing water depth (Table 4). Station I (74 m) showed by far the highest P burial flux with with 0.23 mmol m^{-2} d^{-1}. In contrast the P burial efficiency at this station (Eq. 10) was comparatively low reaching only approximately 26 %. At Station

458 VIII (407 m), the TPP burial flux was 13 mmol m^{-2} d^{-1} and the P burial efficiency exceeded
459 100 % due to the uptake of dissolved P from ambient bottom waters.

460 4.5 Molecular analysis and relative abundance of filamentous sulfur bacteria

461 Molecular analysis indicated the presence of Marithioploca-related bacteria [Salman et al.,
462 2011] in the surface sediments (0-5 cm). Our analysis may, however, underestimate the
463 absolute abundance of these organisms due to a self-splicing mechanism of the 16S rDNA
464 gene [Salman et al., 2012] and is therefore only indicative for their relative abundance.

465 The relative abundance of Marithioploca-related bacteria decreased with increasing water
466 depth (Table 4). Highest relative abundance with more than 4000 copies g^{-1} sediment was
467 found at station I (74 m), decreasing by more than a factor of 20 to 190 copies g^{-1} sediment at
468 station VIII (407 m).

469

470 5 Discussion

471 5.1 POC/xP ratios in water-column particles and sediments

472 In order to characterize the fate of P in oxygen deficient waters and sediments we determined
473 POC/xP ratios from both environments. Previous studies focused either on the water column
474 or on the sediments [Anderson et al., 2001 and references therein; Benitez-Nelson et al., 2004;
475 Faul et al., 2005; Jilbert et al., 2011; Lyons et al., 2011; Sekula-Wood et al., 2012]. The
476 present data set provides a more complete insight into compositional changes and allows us to
477 more rigorously constrain the sedimentary P mass balance compared to earlier studies [Ingall
478 and Jahnke, 1994; Mort et al., 2010; Kraal et al., 2012; Noffke, 2014].].

479 Both water-column particles and the surface sediments from the Peruvian OMZ displayed
480 POC/POP ratios above Redfield, indicating depletion of organic P relative to organic C.
481 Similar observations have been reported before from this and other regions of the ocean [Loh
482 and Bauer, 2000; Benitez-Nelson et al., 2004; Faul et al., 2005; Franz et al., 2012 and others].
483 Preferential remineralization of P phases from sinking particles should lead to increasing
484 POC/POP ratios with increasing water depth, as observed in oxygenated areas of the ocean
485 [reviewed by Ruttenberg, 2014]. However, in the anoxic Cariaco Basin, no such preferential P

mineralization was noted [Benitez-Nelson et al., 2004]. Our results also showed no clear decrease in the POC/POP ratio in the water column, with the possible exception of St. I and VIII. Higher than Redfield POC/POP ratios were observed at Peru on a previous occasion, and may instead be driven by the C-to-P composition of the diatomaceous phytoplankton communities [Franz et al., 2012] rather than preferential P dissolution or other controls such as the input of terrestrial plant material with high POC/POP ratios.

Preferential POP over POC remineralization in anoxic sediments remains controversial [Ingall and Van Cappellen, 1990; Ingall and Jahnke, 1994; Colman et al., 1997; Anderson et al, 2001; McManus et al, 1997; Ruttenberg, 2003; Jilbert et al, 2011]. Our results, however, also showed no clear trend across all stations. At station I, IV and VI (74, 141 and 244m) the POC/POP increased with sediment depth indicating preferential POP over POC remineralization. At station III (128 m) this trend occured only in the upper cm and at station V (195 m) no preferential POP over POC remineralization was found. POC/POP ratios at station VIII (407 m) showed a POP enrichment over the upper 2 cm of the sediment. Below this depth, there was a sudden increase in POC/POP ratios, which is likely due to intense POP remineralization and subsequent authigenic formation of phosphorites (sink-switching, see section 5.2.3).

Another interesting finding pointing to sink-switching can be found in the POC/POP and POC/PIP ratios of the deepest water-column particle sample and the first sediment sample at stations I, IV, VI and VIII (74, 141 and 407 m). Increasing POC/POP and decreasing POC/PIP ratios indicate that POP is converted into PIP while the TPP content of the sediment is conserved (Fig. 2A and B). In agreement with similar findings in anoxic sediments [Ruttenberg and Berner, 1993; Faul et al., 2005 and others] we assume that the observed POP to PIP transformation is due to the formation of CFAs. However, our results emphasize that sink-switching is obviously occurring at the interface between bottom waters and sediments.

Interestingly, the water-column POC/TPP ratios were close to Redfield ratio. This could be an effect of surface adsorption of P on phytoplankton as previously described by Sanudo-Wilhelmy et al. (2004). Those authors investigated different species of *Trichodesmium* from the Atlantic Ocean and found that the intracellular P pool was strongly depleted relative to C, whereas the combination of the intracellular plus the surface adsorbed P was close to the Redfield ratio. Although we did not exactly differentiate between internal and external P

pools, and considering that additional P sources like terrigenous P are negligible (see section 5.2.1), our results generally support the findings of Sanudo-Wilhelmy et al. (2004). However, future studies are required to substantiate this hypothesis.

Sedimentary POC/TPP ratios were also close to Redfield, except at station I and VIII (74 and 407 m). Thus, on the one hand, the sink switching mechanism operates efficiently under low oxygen conditions and on the other hand, the relative degradation of TPP and POC are not changing from the water column to the sediments (Fig. 2B). This is an important finding because at first sight this observation seems to be inconsistent with the long-standing paradigm that low oxygen conditions promote the enhanced release of dissolved P from sediments [Van Cappellen and Ingall, 1996]. However, it should be noted that marine sediments covered by oxygenated bottom waters display molar POC/TPP ratios ranging from about 10 to 50 [Baturin, 2007]. These ratios are much lower than Redfield because P is retained in sediments via adsorption, authigenic mineral precipitation such as Fe (oxyhydr)oxides and microbial P sequestration [Ingall and Jahnke, 1994], and because POC is more efficiently degraded under aerobic conditions [Hedges et al., 1999, Wallmann, 2010]. In contrast, our data set implies that oxygen deficiency causes a shift of POC/TPP ratios to values closer to Redfield compared to oxygenated regions, which is due to both, the enhanced preservation of POC (Dale et al., 2015) and release of dissolved phosphate under low oxygen conditions. It remains puzzling why the extreme P depletion observed in some black shale sequences (e.g. POC/TPP > 3000, Ingall and Jahnke, 1994) are not found in modern anoxic sediments such as those on the Peru margin.

5.2 P mass balance

P release rates from sediments underlying oxygen deficient waters are strongly enhanced compared to oxygenated marine settings, especially in the Peruvian OMZ [Noffke et al., 2012 and 2016]. Nonetheless, the sources for the enhanced P release are still not completely identified. The widely held view is that POP raining from the water column to the sediments represents the main source for sedimentary P in high productive areas like the Peru upwelling system [Delaney, 1998; Filippelli, 2008]. Mass balance approaches that resolve the P regeneration versus burial in oxygen deficient environments by combining sedimentary data and benthic P fluxes are rare [Ingall and Jahnke, 1994; Ingall et al., 2005; Mort et al., 2010; Kraal et al., 2012; Noffke, 2014]. These studies are all based on sediment data only, that is,

548 the external P input to the sediments is estimated or ignored. Furthermore, the study areas
549 were often not covered by fully anoxic bottom waters. Noffke (2014) presented an approach
550 that combines measurements of solid phase P speciation, sediment burial fluxes and benthic
551 chamber flux measurements for a mass balance on benthic P cycling in the Peruvian OMZ.
552 Interestingly, the measurements on the solid phase P speciation revealed that organic P
553 accounted for only 18-37% of the total sedimentary P on the shelf and upper slope [Noffke,
554 2014]. Furthermore, it was found that P bound to Fe (oxyhydr)oxides and terrigenous P was
555 of minor importance for the total sedimentary P inventory. However, authigenic Ca-P with a
556 high amount of fish-P accounted for up to 47% of the total P in sediments down to 300 m
557 water depth and for up to 70% in sediments below 300 m water depth. Consequently, Noffke
558 (2014) suggested that authigenic Ca-P phases are an additional major P source besides
559 organic P for benthic P release in the Peruvian OMZ.

560 Their mass balance approach was solely based on benthic work and has large uncertainties
561 regarding the particulate P input from the water column. Our approach includes the particulate
562 organic and inorganic P input from the water column, benthic P flux measurements and the P
563 burial fluxes and is based on the steady state assumption that the P input has to be sufficient to
564 maintain the benthic P flux and P burial flux. The P mass balance calculations (Table 4)
565 illustrate the variability in TPO_4 release and burial as well as in the magnitude of particulate
566 organic (Fig. 5A) and particulate inorganic P input (Fig. 5B) across the transect. Following
567 the general assumption that POP is the major P phase delivered to the sediments [Delaney,
568 1998; Filippelli, 2008], we first calculated whether the rain rate of POP (RR_{POP}) to the
569 seafloor can account for the measured benthic P fluxes (F_{TPO4}) and P burial fluxes (F_{Pbur}) (Fig.
570 5A, Table 4). However, as already suggested by Noffke et al. (2012 and 2014), the POP
571 fraction is far too small to balance the measured benthic fluxes in the Peruvian OMZ. The
572 POP rain rates calculated along the transect can account for only 25 to 48% of the measured
573 TPO_4 fluxes (Fig. 5A), suggesting the likely presence of an additional inorganic source of
574 dissolved phosphate [Noffke, 2014]. Similar to previous studies [Paytan et al., 2003; Faul et
575 al., 2005; Benitez-Nelson et al., 2007; Lyons et al., 2011; Sekula-Wood et al., 2012], we
576 found that the PIP fraction in water-column particles ranging from 75 to 407 m water depth
577 comprises between 21-74% of TPP (Fig. 3). In the sediments, the average PIP fraction rises to
578 48-98% of TPP (Fig. 3). Furthermore, POC and PIP were correlated (r^2=0.74) in the water-
579 column particles indicating highly reactive material.

The mass balance approach including the PIP rain rate to the seafloor (Fig. 5B) allows the depth transect to be divided into two sections. The transect section I (station I, 74 m and III, 128 m) is characterized by high P input and release rates. The calculations on the P budget show a balance between the particulate P input, the benthic P fluxes and the P burial fluxes within the error margin (± 20%). In transect section II (stations IV, 141 m, V, 195 m and VI, 244 m), the P input decreases drastically (Fig. 5B, Table 4) whereas the benthic P fluxes are still comparatively high. The distinct mismatch in P input and P output prevails as the particulate P rain rates supported only 37 to 53 % of the measured TPO_4 fluxes and calculated burial fluxes. This leads to the question: What drives the excess TPO_4 release in the core of the Peruvian OMZ?

5.2.1 Additional P input

Besides the particulate matter raining to the sediments, other potential other P sources can be considered. Firstly, riverine transported material from the continent may be an additional source of P to the sediments. Due to fast sinking speed and laterally dominated transport it is possible that this P fraction is at least underrepresented on the filter samples. In order to provide a maximum estimate for the contribution of the terrigenous P input to the sediments, this fraction was calculated using the mass accumulation rate of Al in the first centimeter of sediment and an average molar P/Al-ratio (Table 2) of 0.02 for riverine suspended particles [Viers et al., 2009]. The resulting terrigenous P flux accounted for 5-19 % of the total P input, which is insufficient to explain the observed discrepancies in the P budget of transect section II (Table 4, Fig. 4C, 5B).

Laterally transported particles enriched in P from the very shallow shelf could be an additional P source [e.g. Jahnke, 1990]. However, the particles would need to be strongly enriched in P, which is not the case. In addition, this would have to be reflected in the POC/TPP ratios of the surface sediments in transect section II (Fig. 2B). The ratios are not, or only slightly, enriched in TPP compared to the water-column particles, which leadsto the conclusion that lateral transport of P-enriched particles to the sediments is an unlikely candidate for the missing P source.

Another alternative is the existence of an additional PIP phase supplied by fast sinking material (e.g. P containing fish scales; Suess, 1981) that was not sampled during CTD casts, and hence underrepresented on our filter samples. Díaz-Ochoa et al. (2009) showed that fish P

611 can make up to 20% of the total sedimentary P inventory in the shelf sediments of the
612 Peruvian OMZ. Fish P input should be depicted in low sedimentary POC/TPP ratios
613 compared to the water-column particles. Since this difference is not observed it is likely that
614 fish debris can be ruled out for closing the P budget during the sampling campaign.
615 Theoretically, sediments need to be composed of particles having POC/TPP ratios between 11
616 ± 1 and 25 ± 12 (Table 4) to maintain the measured P release rates in transect section II. It
617 seems unlikely that the mismatch in the P mass balance is caused by additional particles
618 deposited at the seabed since their POC/TPP ratio would need to be much lower than any
619 value observed in our data set.

620 **5.2.2 Non steady state scenarios – internal sedimentary P pools**

621 Besides an additional P input to the sediments from the water column, episodic dissolution of
622 particulate P within the sediment could contribute to the excess P release [Noffke et al.,
623 2012]. This could include P solubilized from Fe (oxyhydr)oxides or the degradation of
624 internally stored polyphosphates within sulfide-oxidizing bacteria. Driving factors could
625 include the temporal variability in bottom-water oxygen and nutrient concentrations induced
626 by the passage of internal Kelvin waves and/or interannual variability related to El Niño and
627 La Niña [Guitérrez et al., 2008].

628 It is well recognized that the sedimentary cycles of Fe and P are strongly linked [e.g. Sundby
629 et al., 1986]. Fe (oxyhydr)oxides are expected to be important carriers for phosphorus from
630 the water column to the sediments. Following dissolution of solid Fe minerals in the
631 sediments, the adsorbed P is released to the porewaters. However, in the Peruvian OMZ,
632 oxygen concentrations in the water column are generally below detection limit. Consequently,
633 Fe (oxyhydr)oxides are likely already dissolved in the water column and not such an
634 important P source to the sediments. An estimate of phosphate released during the reduction
635 of Fe (oxyhydr)oxides can be calculated from the diffusive Fe^{2+} fluxes and the molar Fe/P
636 ratio typically found in Fe (oxyhydr)oxides. The diffusive Fe^{2+} fluxes were in the range of 0
637 to 0.03 mmol m^{-2} d^{-1}during the M92 cruise (Table 4) and the molar Fe/P ratio of Fe
638 (oxyhydr)oxides in sediment is around 10 [Slomp et al., 1996]. The calculation of the TPO_4
639 release rates from Fe (oxyhydr)oxides (Eq. 14 in Table 2) results in a flux of 0.003 mmol
640 PO_4^{3-} m^{-2} d^{-1} (Table 4, Fig. 4C and 5B), which is equivalent to less than 5% of the benthic P
641 flux and burial flux.

642 An additional internally activated P pool is phosphate released from large sulfur-oxidizing
643 bacteria, e.g. *Beggiatoa* [Sannigrahi and Ingall, 2005; Brock and Schulz-Vogt, 2011]. These
644 microorganisms store P in the form of intracellular polyphosphate granules when terminal
645 electron acceptors for sulfide oxidation are available (oxic conditions) and release dissolved P
646 during periods when these oxidants are scarce (anoxic conditions). Hence, it is generally
647 assumed that they strongly affect benthic TPO_4 fluxes in a system with frequently changing
648 bottom water redox conditions [Ingall and Jahnke, 1994; Sannigrahi and Ingall, 2005; Schulz
649 and Jørgensen, 2005; Brock and Schulz-Vogt, 2011; Dale et al., 2013].Polyphosphates have
650 been shown to an important P pool in the sediments of highly productive upwelling areas
651 [Kraal et al., 2015]. Along the depth transect at Peru, dense mats of sulfur bacteria related to
652 Marithioploca were observed on the sediments during video-launched MUC and benthic
653 lander deployments down to 300 m water depth [Dale et al., 2015]. Similar findings extended
654 distributions of microbial mats along a latitudinal transect at 11°S off were also previously
655 described by Mosch et al. (2012) and Gutiérrez et al. (2008). Although, these organisms are
656 not known to store polyphosphates like their close relatives, *Beggiatoa* spp. and
657 *Thiomargarita* spp. [Høgslund et al., 2009; Holmkvist et al., 2010], our findings provide
658 circumstantial indications for P uptake and release by Marithioploca-related bacteria.

659 Firstly, we found that the relative abundance of copies of Marithioploca-related bacteria per g^{-1}
660 sediment and the measured benthic TPO_4 release rates correlate linearly (r^2=0.92, Fig. 6).
661 This finding supports the suggestion that bacteria exert an important control on benthic P
662 fluxes. Secondly, a comparison of the in situ measured benthic P fluxes and the diffusive P
663 fluxes calculated from the difference of the TPO_4 bottom water concentration and the TPO_4
664 porewater concentration of the surface sediments revealed large differences (Fig. 4B). Such a
665 difference could be explained by the lysis of bacterial cells during sample retrieval followed
666 by the release of the internally stored polyphosphate pool into the porewater. Following this
667 argument, the diffusive P fluxes cannot be taken as real fluxes, but as a measure for potential
668 maximum release rates of P by Marithioploca-related bacteria. It should be noted that, the
669 potential fluxes are more than sufficient to compensate for the missing P fraction in transect
670 section II (ranging from 0.5 to 1.6 mmol m^{-2} d^{-1}; Table 4, Fig. 4B).

671 In addition to the established porewater extraction procedure, we carried out freeze/thaw
672 experiments to quantify the amount of P stored in sulfide-oxidizing bacteria (see method
673 section 3.7). The released polyphosphates from the microbial cells after repeated freeze/thaw

674 cycles are rapidly hydrolyzed to orthophosphate under acidic conditions [Jager and Heyns,
675 1998]. Hence, the standard method to determine phosphate in the porewaters using acidic
676 reagents will favor the hydrolysis of polyphosphates enabling us the measure its concentration
677 in the porewaters after conducting the experiments. However, this method cannot exclude P
678 release from other bacteria and, possibly, foraminifera in the sediments. A comparison of the
679 porewater phosphate concentrations and the experiment results shows that the amount of the
680 internal P reservoir is as twice as high as the porewater P concentration in transect section I
681 and more than ten times higher in section II (Fig. 7). These results are coincident with the
682 findings from the mass balance approach, where the largest discrepancies occur in transect
683 section II and are another indication for the bacterial impact on the benthic P release.
684 Interestingly, the highest phosphate concentrations after the freeze/thaw experiments were
685 found at station VIII (407 m) with abundant foraminifera rather than sulfide-oxidizing
686 bacteria. Hence, we assume that the sulfide-oxidizing bacteria at station IV, V and VI (141,
687 194 and 244 m) and, potentiallay, the foraminifera observed at station VIII (407 m) are
688 contributing phosphate to the porewaters. To our knowledge, P storage by foraminifera has
689 not been demonstrated previously and awaits further study.

690 It remains to be shown how these mechanisms play out in detail (e.g. nutrient concentration
691 thresholds, P uptake and release time scalesyby Marithioploca-related bacteria) and how they
692 impact benthic P release in oxygen and nitrate deficient environments on longer time scales.
693 Summarizing the results of the mass balance, it should be noted, that, even with the relevant
694 data on particulate P rain rates, the benthic P mass balance for the core of the Peruvian OMZ
695 is imbalanced and requires an additional P source to maintain the benthic TPO_4 fluxes. We
696 suggest that sulfur bacteria make an important contribution to this missing P source.

697 ### 5.2.3 Indications for active phosphorite formation

698 In contrast to the stations between 74 and 244 m water depth characterized by P release, data
699 from station VIII at 407 m water depth indicate the uptake of phosphate from the bottom
700 water. To our best knowledge, this is the first time that a downward flux of dissolved
701 phosphate from bottom waters into phosphorite-bearing surface sediments has been
702 documented by in situ benthic flux measurements. Furthermore, the PIP concentrations in the
703 surface sediments of station VIII (Fig. 2a) were 10 to 60 times higher compared to the
704 shallower stations where P was released from the sediments. Taken together, these

observations indicate that a PIP phase, likely phosphorite, is precipitating from the porewater phosphate at the time of sampling. This is also reflected in decreasing porewater phosphate concentrations (Fig. 7).

Arning et al. (2008) presented investigations on phosphorites recovered from the Peruvian OMZ including a station at 12°S from the same water depth (~ 400 m) close to sampling station VIII. The suboxic bottom waters and low sedimentation rates in that area seem to be favorable for phosphorite formation close to the sediment-water interface [Arning et al., 2009b]. Cosmidis et al. (2013) suggested three mechanisms how high porewater phosphate concentrations that are essential for the phosphogenesis can be generated in the sediments: (1) remineralization of organic matter mainly through bacterial sulfate reduction releasing phosphate to the porewaters, (2) reductive dissolution of Fe (oxyhydr)oxides and the release of adsorbed P and (3) synthesis of internally stored polyphosphates by large sulfide-oxidizing bacteria. Using the same mass balance approach as presented before, we calculate a P accumulation rate of 33 ± 4 mmol m^{-2} yr^{-1} at station VIII where most of the P is derived from ambient bottom waters (26 mmol m^{-2} yr^{-1}). Hence, our data suggest that the phosphorite nodules at this station contain phosphate that originates predominantly from ambient bottom waters. Additionally, as already mentioned, sediments at station VIII were covered by benthic foraminifera instead of mat-forming sulfur bacteria. The release of phosphate from frozen samples from this site may indicate that these foraminifera are a source for polyphosphates (see section 3.7 and Fig. 7). Our observations suggest that benthic foraminifera rather than bacterial mats might facilitate the uptake of bottom water phosphate and the formation of phosphorites at this station. However, this remains an open question and should be addressed in future field campaigns.

The P uptake rate of ~ 26 mmol P m^{-2} yr^{-1} derived from our lander measurements may be compared to previous estimates on phosphorite growth rates in the area. Dating of phosphoric laminites yields a P uptake rate of only 3 mmol P m^{-2} yr^{-1} for a ca. 1 Ma old nodule [Arning et al., 2009a]. These different fluxes may be at least partly explained by the methodological difference (present flux measurement vs. long-term average). However, growth rates determined on modern nodules are broadly consistent with our flux measurements [Burnett et al., 1982].

6 Conclusions

This study aimed to identify the P sources of benthic P release in the Peruvian OMZ. We determined the rain rates of particulate organic phosphorus and particulate inorganic phosphorus as well as benthic P release rates and P burial fluxes.

Our calculations revealed that within the core OMZ particulate phosphorus rain rates cannot account for measured benthic P fluxes and burial fluxes. From systematic analysis of potential P sources, we conclude that periodic P release from sulfur bacteria that store and release P under oscillation redox conditions could strongly modulate benthic P fluxes, and hence explain for the missing P source. We visited the area during austral summer when oxygen and nitrate levels were depleted by high export production and respiration. It is possible that the Peruvian OMZ was less reducing prior to our sampling period due to lower respiration rates and/or better ventilation. Thus, we propose that the bacterial mats on the Peruvian margin act as phosphorus capacitors being, discharged during austral summer and recharged during other periods of the year when bottom waters are less reducing, as previously proposed in Dale et al. (2013). This hypothesis could be tested by studying the seasonality of benthic fluxes in the Peruvian up-welling system and P dynamics within the bacterial community.

In addition, measurements at one station (407 m water depth) showed clear indications for the uptake of dissolved phosphate by the sediments facilitating phosphorite formation. Our data imply that most of the P accumulating in these authigenic minerals originates from ambient bottom waters. Since this site was marked by a high abundance of benthic foraminifera, we speculate that phosphate uptake and phosphorite formation may be linked to the presence of these organisms. This requires further stuy.

There was no clear preferential mineralization of POP relative to POC with depth in the water column. POC/TPP ratios in both water-column particles and sediments were close to Redfield at most sites in the Peruvian OMZ. This observation strongly suggests that the relative burial efficiencies of POC and TPP are similar under low oxygen conditions. Importantly, it further shows that the sediments underlying the anoxic waters on the Peru margin are not depleted in P compared to Redfield. Rather, they are depleted relative to sediments underlying oxic waters, which show POC/TPP ratios well below Redfield [Wallmann, 2010]. Thus, at Peru, a lack of oxygen promotes the intensified release of dissolved P from sediments, whilst preserving a POC/TPP burial ratio that issimilar to Redfield.

Our data support the hypothesis that benthic P release is linked via a positive feedback loop to intensified primary production in the surface water and oxygen demand in the water column during periods where bottom water redox conditions promote the release of P from the sediments. However, this positive feedback is limited by the formation of authigenic inorganic P phases that maintains the long-term average POC/TPP burial ratio close to Redfield.

Author contribution

UL, AD and SS supported the shipboard work, geochemical analysis and contributed to the manuscript. CH, KW and AN helped with fruitful discussions related to the manuscript and helped with the manuscript preparation. CL carried out the molecular analysis and contributed to the manuscript.

Acknowledgements

We are very grateful to the crew of RV *Meteor* during cruise M92 for the support of. Our thanks also go to A. Petersen, M. Türk and S. Cherednichenko for their assistance in deploying the landers. For their enthusiastic help and cooperation, we thank B. Domeyer, S. Kriwanek, A. Bleyer, R. Suhrberg, S. Trinkler and V. Thoenissen for biogeochemical analyses on board and in the home laboratory. Furthermore, we appreciate Christopher Voigt from the University of Bremen for carrying out XRD analysis. This work is a contribution of the Sonderforschungsbereich 754 "Climate – Biogeochemistry Interactions in the Tropical Ocean" (www.sfb754.de) which is supported by the Deutsche Forschungsgemeinschaft.

References

Anderson, L. D., Delaney, M. L., and Faul, K. L.: Carbon to phosphorus ratios in sediments: Implications for nutrient cycling, Global Biogeochemical Cycles, 15(1), 65-79, 2001.

Arning, E. T., Birgel, D., Schulz-Vogt, H. N., Holmkvist, L., Jørgensen, B. B., Larson, A., and Peckmann, J.: Lipid Biomarker Patterns of Phosphogenic Sediments from Upwelling Regions, Geomicrobiology Journal, 25(2), 69-82, 2008.

Arning, E. T., Birgel, D., Brunner, B., and Peckmann, J.: Bacterial formation of phosphatic laminites off Peru, Geobiology, 7(3), 295-307, 2009a.

Arning, E. T., Lückge, A., Breuer, C., Gussone, N., Birgel, D., and Peckmann, J.: Genesis of phosphorite crusts off Peru, Marine Geology, 262(1–4), 68-81, 2009b.

Asahi, T., Ichimi, K., Yamaguchi, H., and Tada, K.: Horizontal distribution of particulate matter and its characterization using phosphorus as an indicator in surface coastal water, Harima-Nada, the Seto Inland Sea, Japan, Journal of Oceanography, 70(3), 277-287, 2014.

Aspila, K. I., Agemian, H., and Chau, A. S. Y.: A semi-automated Method for the Determination of Inorganic, Organic and Total Phosphate in Sediments, Analyst, 101, 187-197, 1976.

Baturin, G. N.: Issue of the relationship between primary productivity of organic carbon in ocean and phosphate accumulation (Holocene– Late Jurassic), Lithol. Miner. Resour., 42(4), 318–348, 2007, doi:10.1134/ S0024490207040025.

Benitez-Nelson, C. R.: The biogeochemical cycling of phosphorus in marine systems, Earth-Science Reviews, 51(1–4), 109-135, 2000.

Benitez-Nelson, C. R., O'Neill, L., Kolowith, L. C., Pellechia, P., and Thunell, R.: Phosphonates and particulate organic phosphorus cycling in an anoxic marine basin, Limnol. Ocean., 49(5), 1593-1604, 2004.

Benitez-Nelson, C. R., O'Neill Madden, L. P., Styles, R. M., Thunell, R. C., and Astor, Y.: Inorganic and organic sinking particulate phosphorus fluxes across the oxic/anoxic water column of Cariaco Basin, Venezuela, Marine Chemistry, 105(1–2), 90-100, 2007.

817 Bertics, V. J., Löscher, C. R., Salonen, I., Dale, A. W., Gier, J., Schmitz, R. A., and Treude,
818 T.: Occurrence of benthic microbial nitrogen fixation coupled to sulfate reduction in the
819 seasonally hypoxic Eckernförde Bay. Baltic Sea. Biogeosciences. 10, 1243-1258, 2013.

820 Boudreau, B. P.: The diffusive tortuosity of fine-grained unlithified sediments. Geochim.
821 Cosmochim. Acta 60, 3139–3142, 1996.

822 Brock, J., and Schulz-Vogt, H. N.: Sulfide induces phosphate release from polyphosphate in
823 cultures of a marine Beggiatoa strain, ISME J, 5(3), 497-506, 2011.

824 Burnett, W. C., Beers, M. J., and Roe, K. K.: Growth Rates of Phosphate Nodules from the
825 Continental Margin Off Peru, Science, 215(4540), 1616-1618, 1982.

826 Colman, A. S., Mackenzie, F. T., and Holland, H. D.: Redox Stabilization of the Atmosphere
827 and Oceans and Marine Productivity. Science 275, 406-408. 1997.

828 Compton, J., Mallinson, D., Glenn, C., Filippelli, G., Föllmi, K., Shields, G., and Zanin, Y.:
829 Variations in the global phosphorus cycle, in Marine authigenesis: from global to microbial,
830 SEPM (Society for Sedimentary Geology), 21-33, 2000.

831 Cosmidis, J., Benzerara, K., Menguy, N., and Arning, E.: Microscopy evidence of bacterial
832 microfossils in phosphorite crusts of the Peruvian shelf: Implications for phosphogenesis
833 mechanisms, Chemical Geology, 359, 10-22, 2013.

834 Dale, A., Bertics, W., V. J., Treude, T., Sommer, S., and Wallmann, K.: Modeling benthic–
835 pelagic nutrient exchange processes and porewater distributions in a seasonally hypoxic
836 sediment: evidence for massive phosphate release by *Beggiatoa*? Biogeosciences 10, 629-651,
837 2013.

838 Dale, A. W., Sommer, S., Lomnitz, U., Montes, I., Treude, T., Liebetrau, V., Gier, J., Hensen,
839 C., Dengler, M., Stolpovsky, K., Bryant, L. D., and Wallmann, K.: Organic carbon
840 production, mineralisation and preservation on the Peruvian margin, Biogeosciences, 12(5),
841 1537-1559, 2015.

842 Delaney, M. L.: Phosphorus accumulation in marine sediments and the oceanic phosphorus
843 cycle, Global Biogeochemical Cycles, 12(4), 563-572, 1998.

844 Díaz-Ochoa, J. A., Lange, C. B., Pantoja, S., De Lange, G. J., Gutierrez, D., Munoz, P., and
845 Salamanca M.: Fish scales in sediments from off Callao, central Peru, Deep-Sea Res. Part II-
846 Top. Stud. Oceanogr., 56(16), 1113-1124, 2009.

847 Faul, K. L., Paytan, A., and Delaney, M. L.: Phosphorus distribution in sinking oceanic
848 particulate matter, Marine Chemistry, 97(3–4), 307-333, 2005.

849 Filippelli, G. M.: The global phosphorus cycle, in Phosphates: Geochemical, Geobiological,
850 and Materials Importance, edited by M. Kohn, J. Rakovan and J. Hughes, pp. 391-425,
851 Reviews in Mineralogy&Geochemistry, 2002.

852 Filippelli, G. M.:The Global Phosphorus Cycle: Past, Present, and Future, Elements, 4(2), 89-
853 95, 2008.

854 Föllmi, K. B.: The phosphorus cycle, phosphogenesis and marine phosphate-rich deposits,
855 Earth-Science Reviews, 40(1–2), 55-124, 1996.

856 Franz, J., Krahmann, G., Lavik, G., Grasse, P., Dittmar, T., and Riebesell, U.: Dynamics and
857 stoichiometry of nutrients and phytoplankton in waters influenced by the oxygen minimum
858 zone in the eastern tropical Pacific, Deep Sea Research Part I: Oceanographic Research
859 Papers, 62(0), 20-31, 2012.

860 Froelich, P. N., Arthur, M. A., Burnett, W. C., Deakin, M., Hensley, V., Jahnke, R., Kaul, L.,
861 Kim, K. H., Roe, K., Soutar, A., Vathakanon, C.: Early diagenesis of organic matter in Peru
862 continental margin sediments: Phosphorite precipitation, Marine Geology, 80(3–4), 309-343,
863 1988.

864 Fuenzalida, R., Schneider, W., Garcés-Vargas, J., Bravo, L., and Lange, C.: Vertical and
865 horizontal extension of the oxygen minimum zone in the eastern South Pacific Ocean, Deep
866 Sea Research Part II: Topical Studies in Oceanography, 56(16), 992-1003, 2009.

867 Ganeshram, R. S., Pedersen, T. F., Calvert, S., and Francois, R.: Reduced nitrogen fixation in
868 the glacial ocean inferred from changes in marine nitrogen and phosphorus inventories,
869 Nature, 415(6868), 156-159, 2002.

870 Glenn, C. R., and Arthur, M. A.: Petrology and major element geochemistry of Peru margin
871 phosphorites and associated diagenetic minerals: Authigenesis in modern organic-rich
872 sediments, Marine Geology, 80(3–4), 231-267, 1988.

873 Goldhammer, T., Bruchert, V., Ferdelman, T. G., and Zabel, M.: Microbial sequestration of
874 phosphorus in anoxic upwelling sediments, Nature Geosci, 3(8), 557-561, 2010.

875 Govindaraju K.: Compilation of working values and sample description for 383 geostandards.
876 Geostandard Newslett. 18, 1–158, 1994.

877 Graco, M., Purca, S., Dewitte, B., Morón, O., Ledesma, J., Flores, G., Castro, C., and
878 Gutiérrez, D.: The OMZ and nutrients features as a signature of interannual and low
879 frequency variability off the peruvian upwelling system, Biogeosciences Discuss., 2016, 1-36,
880 2016.

881 Grasshoff, K., Erhardt, M., Kremling, K.: Methods of seawater analysis, 3rd ed. Wiley-VCH
882 (1999).

883 Gutiérrez, D., Enríquez, E., Purca, S., Quipúzcoa, L., Marquina, R., Flores, G., and Graco,
884 M.: Oxygenation episodes on the continental shelf of central Peru: Remote forcing and
885 benthic ecosystem response, Progress in Oceanography, 79(2–4), 177-189, 2008.

886 Hedges, J. I., Hu, F. S., Devol, A. H., Hartnett H. E., Tsamakis, E. and Keil, R. G.:
887 Sedimentary organic matter preservation: A test for selective degradation under oxic
888 conditions. American Journal of Science 299, 529-555. 1999.

889 Høgslund, S., Revsbech, N. P., Kuenen, J. G., Jorgensen, B. B., Gallardo, V. A., Vossenberg,
890 J. v. d., Nielsen, J. L., Holmkvist, L., Arning, E. T., and Nielsen, L. P.: Physiology and
891 behaviour of marine Thioploca, ISME J, 3(6), 647-657, 2009.

892 Holmkvist, L., Arning, E. T., Küster-Heins, K., Vandieken, V., Peckmann, J., Zabel, M., and
893 Jørgensen, B. B.: Phosphate geochemistry, mineralization processes, and Thioploca
894 distribution in shelf sediments off central Chile, Marine Geology, 277(1–4), 61-72, 2010.

895 Ingall, E. D., and Van Cappellen P.: Relation between sedimentation rate and burial of
896 organic phosphorus and organic carbon in marine sediments, Geochimica et Cosmochimica
897 Acta, 54(2), 373-386, 1990.

898 Ingall, E., and Jahnke R.: Evidence for enhanced phosphorus regeneration from marine
899 sediments overlain by oxygen depleted waters, Geochimica et Cosmochimica Acta, 58(11),
900 2571-2575, 1994.

901 Ingall, E., and R. Jahnke: Influence of water-column anoxia on the elemental fractionation of
902 carbon and phosphorus during sediment diagenesis, Marine Geology, 139(1–4), 219-229,
903 1997.

904 Ingall, E., Kolowith, L., Lyons, T., and Hurtgen, M.: Sediment carbon, nitrogen and
905 phosphorus cycling in an anoxic fjord, Effingham Inlet, British Columbia, American Journal
906 of Science, 305(3), 240-258, 2005.

907 Ingall, E. D.: Biogeochemistry: Phosphorus burial, Nature Geosci, 3(8), 521-522, 2010.

908 de Jager, H.-J., and Heyns, A. M.: Kinetics of Acid-Catalyzed Hydrolysis of a Polyphosphate
909 in Water, The Journal of Physical Chemistry A, 102(17), 2838-2841, 1998.

910 Jahnke, R. A.: Early diagenesis and recycling of biogenic debris at the seafloor, Santa Monica
911 Basin, California, Journal of Marine Research, 48(2), 413-436, 1990.

912 Jilbert, T., Slomp, C. P., Gustafsson, B. G., and Boer W.: Beyond the Fe-P-redox connection:
913 preferential regeneration of phosphorus from organic matter as a key control on Baltic Sea
914 nutrient cycles, Biogeosciences, 8(6), 1699-1720, 2011.

915 Kraal, P., Slomp, C. P., Reed, D. C, Reichart, G.-J., and Poulton, S. W.: Sedimentary
916 phosphorus and iron cycling in and below the oxygen minimum zone of the northern Arabian
917 Sea, Biogeosciences, 9(7), 2603-2624, 2012.

918 Kraal, P., Bostick, B. C., Behrends, T., Reichart, G.-J., and Slomp, C. P.: Characterization of
919 phosphorus species in sediments from the Arabian Sea oxygen minimum zone: Combining
920 sequential extractions and X-ray spectroscopy, Marine Chemistry, 168(0), 1-8, 2015.

921 Krissek, L. A., Scheidegger, K. F., and Kulm, L. D.: Surface sediments of the Peru-Chile
922 continental margin and the Nazca plate, Geological Society of America Bulletin, 91(6), 321-
923 331, 1980.

924 Li, Y.-H. and Gregory, S.: Diffusion of ions in sea water andin deep-sea sediments. Geochim.
925 Cosmochim. Acta 38, 703–714, 1974.

926 Loh, A. N., and Bauer, J. E.: Distribution, partitioning and fluxes of dissolved and particulate
927 organic C, N and P in the eastern North Pacific and Southern Oceans, Deep Sea Research Part
928 I: Oceanographic Research Papers, 47(12), 2287-2316, 2000.

929 Löscher, C. R., Kock, A., Könneke, M., LaRoche, J., Bange, H. W., and Schmitz, R. A.:
930 Production of oceanic nitrous oxide by ammonia-oxidizing archaea. Biogeosciences. 9. 2419-
931 2429, 2012.

932 Lyons, G., Benitez-Nelson, C. R., and Thunell, R. C.: Phosphorus composition of sinking
933 particles in the Guaymas Basin, Gulf of California, Limnology and Oceanography, 56(3),
934 1093-1105, 2011.

935 McManus, J., Berelson, W. M., Coale, K. H., Johnson, K. S., and Kilgore, T. E.: Phosphorus
936 regeneration in continental margin sediments, Geochimica et Cosmochimica Acta, 61(14),
937 2891-2907, 1997.

938 Moffitt, S. E., Moffitt, R. A., Sauthoff, W., Davis, C. V., Hewett, K., and Hill T. M.:
939 Paleoceanographic Insights on Recent Oxygen Minimum Zone Expansion: Lessons for
940 Modern Oceanography, PLoS ONE, 10(1), 2015.

941 Mort, H. P., Slomp, C. P., Gustafsson, B. G., and Andersen, T. J.: Phosphorus recycling and
942 burial in Baltic Sea sediments with contrasting redox conditions, Geochimica et
943 Cosmochimica Acta, 74(4), 1350-1362, 2010.

944 Mosch, T., Sommer, S., Dengler, M., Noffke, A., Bohlen, L., Pfannkuche, O., Liebetrau, V.,
945 and Wallmann, K.: Factors influencing the distribution of epibenthic megafauna across the
946 Peruvian oxygen minimum zone, Deep Sea Research Part I: Oceanographic Research Papers,
947 68(0), 123-135, 2012.

948 Noffke A., Hensen, C., Sommer, S., Scholz, F., Bohlen L., Mosch, T., Graco M., and
949 Wallmann K.: Benthic iron and phosphorus fluxes across the Peruvian oxygen minimum
950 zone, Limnology and Oceanography, 57(3), 851-867, 2012.

951 Noffke A.: Phosphorus cycling in anoxic sediments, PhD dissertation, University of Kiel,
952 2014.

953 Noffke, A., Sommer, S., Dale, A.W., Hall, P.O.J., and Pfannkuche, O.: Benthic nutrient fluxes
954 in the Eastern Gotland Basin (Baltic Sea) with particular focus on microbial mat ecosystems,
955 Journal of Marine Systems, 2016, doi: 10.1016/j.jmarsys.2016.01.007.

956 Paytan, A., Cade-Menun, B. J., McLaughlin, K., and Faul, K. L.: Selective phosphorus
957 regeneration of sinking marine particles: evidence from 31P-NMR, Marine Chemistry, 82(1–
958 2), 55-70, 2003.

959 Paytan, A., and McLaughlin, K.: The Oceanic Phosphorus Cycle, Chemical Reviews, 107(2),
960 563-576, 2007.

961 Pennington, J. T., Mahoney, K. L., Kuwahara, V. S., Kolber, D. D., Calienes, R., and Chavez,
962 F. P.: Primary production in the eastern tropical Pacific: A review, Progress in Oceanography,
963 69(2–4), 285-317, 2006.

964 Redfield, A. C., Ketchum, B. H., and Richards, F. A.: The influence of organisms on the
965 composition of seawater, in The Sea, Academic Press, London, 26-77, 1963.

966 Reimers, C. E., and Suess, E.: Spatial and temporal patterns of organic matter accumulation
967 on the Peru continental margin, in Coastal Upwelling: Part B. Sedimentary Record of Ancient
968 Coastal Upwelling, edited by E. Suess and J. Thiede, pp. 311-346, Plenum Press, New York,
969 1983.

970 Roth, R., S. P. Ritz, S. P. and Joos, F.: Burial-nutrient feedbacks amplify the sensitivity of
971 atmospheric carbon dioxide to changes in organic matter remineralisation. Earth Syst.
972 Dynam., 5, 321-343, 2014, doi:10.5194/esd-5-321-2014.

973 Ruttenberg, K. C., and Berner, R. A.: Authigenic apatite formation and burial in sediments
974 from non-upwelling, continental margin environments, Geochimica et Cosmochimica Acta,
975 57(5), 991-1007, 1993.

976 Ruttenberg, K. C.: The Global Phosphorus Cycle, In: Treatise on Geochemistry, Turekian
977 K.K. and Holland D.J., (eds), Elsevier, 585–643, 2003.

978 Ruttenberg, K. C.: The Global Phosphorus Cycle. In Treatise on Geochemistry, H. D. Holland
979 and K. K. Turekian (eds), Elsevier, 499-558, 2014.

980 Salman, V., Amann R., Girnth A.-C., Polerecky L., Bailey J. V., Høgslund S., Jessen G.,
981 Pantoja S., and Schulz-Vogt H. N.: A single-cell sequencing approach to the classification of
982 large, vacuolated sulfur bacteria, Systematic and Applied Microbiology, 34(4), 243-259,
983 2011.

984 Salman, V., Amann, R, Shub, D. A., Schulz-Vogt, H. N.: Multiple self-splicing introns in the
985 16S rRNA genes of giant sulfur bacteria, PNAS, 109(11), 4203-4208, 2012,
986 doi:10.1073/pnas.1120192109.

987 Sannigrahi, P., and Ingall, E.: Polyphosphates as a source of enhanced P fluxes in marine
988 sediments overlain by anoxic waters: Evidence from 31P NMR, Geochemical Transactions,
989 6(3), 52, 2005.

990 Sanudo-Wilhelmy, S. A., Tovar-Sanchez, A., Fu, F.-X., Capone, D. G., Carpenter, E. J., and
991 Hutchins, D. A.: The impact of surface-adsorbed phosphorus on phytoplankton Redfield
992 stoichiometry, Nature, 432(7019), 897-901, 2004.

993 Schenau, S. J., and De Lange, G. J.: A novel chemical method to quantify fish debris in
994 marine sediments, Limnology and Oceanography, 45(4), 963-971, 2000.

995 Schenau, S. J., and De Lange, G. J.: Phosphorus regeneration vs. burial in sediments of the
996 Arabian Sea, Marine Chemistry, 75(3), 201-217, 2001.

997 Scholz, F., Hensen, C., Noffke, A., Rohde, A., Liebetrau, V., and Wallmann, K.: Early
998 diagenesis of redox-sensitive trace metals in the Peru upwelling area – response to ENSO-
999 related oxygen fluctuations in the water column, Geochimica et Cosmochimica Acta, 75(22),
1000 7257-7276, 2011.

1001 Schulz, H. N., and Jørgensen, B. B.: Thiomargarita, In Krieg, N. R., J. T. Staley, and D. J.
1002 Brenner (ed), Bergey's Manual of Determinative Bacteriology, Vol. 2, part B, Springer-
1003 Verlag, Berlin, Heidelberg, New York, 2005.

1004 Schulz, H. N., and Schulz, H. D.: Large Sulfur Bacteria and the Formation of Phosphorite,
1005 Science, 307(5708), 416-418, 2005.

1006 Schunck, H., Lavik, G., Desai, D. K., Großkopf, T., Kalvelage, T., Löscher, C. R., Paulmier,
1007 A., Contreras, S., Siegel, H., Holtappels, M., Rosenstiel, P., Schilhabel, M. B., Graco, M.,
1008 Schmitz, R. A., Kuypers, M. M. M., and LaRoche, J.: Giant Hydrogen Sulfide Plume in the
1009 Oxygen Minimum Zone off Peru Supports Chemolithoautotrophy, PLoS ONE 8(8), 2013.

1010 Sekula-Wood, E., Benitez-Nelson, C. R., Bennett, M. A., and Thunell R.: Magnitude and
1011 composition of sinking particulate phosphorus fluxes in Santa Barbara Basin, California,
1012 Global Biogeochemical Cycles, 26(2), GB2023, 2012.

1013 Slomp, C. P., Van der Gaast, S. J., and Van Raaphorst, W.: Phosphorus binding by poorly
1014 crystalline iron oxides in North Sea sediments, Marine Chemistry, 52(1), 55-73, 1996.

1015 Slomp, C. P., Malschaert, J. F. P., and Van Raaphorst, W.: The role of adsorption in
1016 sediment-water exchange of phosphate in North Sea continental margin sediments, Limnol.
1017 Ocean., 43(5), 832-846, 1998.

1018 Slomp, C. P., and Van Cappellen, P.: The global marine phosphorus cycle: sensitivity to
1019 oceanic circulation, Biogeosciences, 4(2), 155-171, 2007.

1020 Sommer, S., Linke, P., Pfannkuche, O., Schleicher, T., v. Deimling, S., Reitz, A., Haeckel,
1021 M., and Hensen, C.: Seabed methane emissions and the habitat of frenulate tubeworms on the
1022 Captain Arutyunov mud volcano (Gulf of Cadiz), Marine Ecology Progress Series, 382, 69-
1023 86, 2009.

1024 Sommer, S., Gier, J., Treude, T., Lomnitz, U., Dengler, M., Cardich, J. and Dale, A.:
1025 Depletion of oxygen, nitrate and nitrite in the Peruvian oxygen minimum zone cause an
1026 imbalance of benthic nitrogen fluxes. Deep-Sea Research Part I, submitted, 2015.

1027 Stramma, L., Johnson, G. C., Sprintall, J., and Mohrholz, V.: Expanding Oxygen-Minimum
1028 Zones in the Tropical Oceans, Science, 320(5876), 655-658, 2008.

1029 Strub, P. T., Mesias, J. M., Montecino, V., Ontecino, R., and Salinas S.: Coastal ocean
1030 circulation of western South. America, in The Sea, edited by A. R. R. a. K. H. Brink, pp. 273–
1031 313, Wiley, 1998.

1032 Suess, E.: Phosphate regeneration from sediments of the Peru continental margin by
1033 dissolution of fish debris, Geochimica et Cosmochimica Acta, 45(4), 577-588, 1981.

1034 Suess, E., Kulm, L. D., and Killingley, J. S.: Coastal upwelling and a history of organic rich
1035 mudstone deposition off Peru., in Marine Petroleum Source rocks, edited by J. Brooks and A.
1036 J. Fleet, pp. 1129-1145, Geological Society Spec, 1987.

1037 Suess, E., and von Huene, R.: Ocean Drilling Program Leg 112, Peru continental margin: Part
1038 2, Sedimentary history and diagenesis in a coastal upwelling environment, Geology, 16(10),
1039 939-943, 1988.

1040 Sundby, B., Anderson, L. G., Hall, P. O. J., Iverfeldt, Å., van der Loeff, M. M. R., and
1041 Westerlund, S. F. G.: The effect of oxygen on release and uptake of cobalt, manganese, iron
1042 and phosphate at the sediment-water interface, Geochimica et Cosmochimica Acta, 50(6),
1043 1281-1288, 1986.

1044 Tamura K., Stecher, G., Peterson, D., Filipski, A. and Kumar, S.: MEGA6, Molecular
1045 Evolutionary Genetics Analysis Version 6.0. Molecular Biology and Evolution 30: 2725-
1046 2729, 2013.

1047 Teske, A., Ramsing, N. B., Küver, J., and Fossing, H.: Phylogeny of Thioploca and Related
1048 Filamentous Sulfide-Oxidizing Bacteria, Systematic and Applied Microbiology, 18(4), 517-
1049 526, 1995.

1050 Tsandev, I., Reed, D. C., and Slomp, C. P.: Phosphorus diagenesis in deep-sea sediments:
1051 Sensitivity to water column conditions and global scale implications, Chemical Geology,
1052 330–331(0), 127-139, 2012.

1053 Van Cappellen, P., and Ingall, E. D.: Redox Stabilization of the Atmosphere and Oceans by
1054 Phosphorus-Limited Marine Productivity, Science, 271(5248), 493-496, 1996.

1055 Viers, J., Dupré, B., and Gaillardet, J.: Chemical composition of suspended sediments in
1056 World Rivers: New insights from a new database, Science of The Total Environment, 407(2),
1057 853-868, 2009.

1058 Wallmann, K.: Feedbacks between oceanic redox states and marine productivity: A model
1059 perspective focused on benthic phosphorus cycling, Global Biogeochemical Cycles, 17(3),
1060 2003.

1061 Wallmann, K.: Phosphorus imbalance in the global ocean?, Global Biogeochemical Cycles,
1062 24(4), 2010.

Tables

Table 1: Station list for the sites of the benthic lander (BIGO), multi-corer (MUC) and CTD deployments including the bottom water concentrations of oxygen (O_2), nitrate (NO_3^-) and sulfide (H_2S) in µM. The station numbers were according to Dale et al., 2015. bdl=below detection limit (5 µM)

Nr.	Station	Gear	Date (2013)	Longitude (°W)	Latitude (°S)	Water depth (m)	BW O_2 (µM)	BW NO_3^- (µM)	BW H_2S (µM)
	98	CTD26	14.01.	12°13.504’	77°10.799’	75			
I	220	MUC39	25.01.	12°13.531’	77°10.061’	72	bdl	-	33.22
	110	BIGO1-2	15.01.	12°13.506’	77°10.793’	74			
	269	CTD79	29.01.	12°16.690’	77°14.999’	128			
III	248	MUC46	27.01.	12°16.697’	77°15.001’	129	bld	0.02	-
	165	BIGO2-4	20.01.	12°16.690’	77°14.995’	128			
	111	CTD29	15.01.	12°18.729’	77°17.757’	145			
IV	36	MUC10	09.01.	12°18.708’	77°17.794	145	bdl	7.1	
	57	BIGO1-1	11.01.	12°18.711’	77°17.803’	141			
	279	CTD81	30.01.	12°21.490’	77°21.713’	195			
V	247	MUC45	27.01.	12°21.491’	77°21.702’	195	bdl	6.3	-
	201	BIGO1-4	23.01.	12°21.502’	77°21.712’	195			
	92	CTD24	13.01.	12°23.300’	77°24.200’	244			
VI	198	MUC34	23.01.	12°23.300’	77°24.228’	244	bdl	11.9	-
	74	BIGO2-2	12.01.	12°23.300’	77°24.186’	244			

	66	CTD16	12.01.	12°27.535’	77°29.593	414			
VIII	107	MUC23	15.01.	12°27.198’	77°29.497’	407	bdl	12.1	-
	207	BIGO2-5	24.01.	12°27.207'	77°29.517'	409			

1067

1068 **Table 2:** Equations for the P mass balance calculations. Results are shown in Table 4.

Equations for P mass balance calculations		
P Input to the sediments (mmol m^{-2} d^{-1})		
(4)	Total particulate phosphorus rain rate	$RR_{TPP} = RR_{PIP} + RR_{POP} = F_{TPO4} + F_{Pbur}$
(5)	Particulate inorganic phosphorus rain rate	$RR_{PIP} = RR_{POC} / \left(\frac{POC}{PIP}\right)$
(6)	Particulate organic phosphorus rain rate	$RR_{POP} = RR_{POC} / \left(\frac{POC}{POP}\right)$
(7)	Terrigenous P input (P/Al = 0.02, Vier et al., 2009)	$RR_{Pterr} = Al_{(0-1)} * MAR * \frac{P}{Al}$
P Burial in the sediments (mmol m^{-2} d^{-1} and g m^{-2} d^{-1}) at 11 cm		
(8)	Phosphorus burial flux	$F_{Pbur} = MAR * P_{11}$
(9)	Mass accumulation rate	$MAR = \rho_{dry} * (1 - \phi_{\infty}) * SR$
(10)	TPP burial efficiency	$PBE = MAR * \left(\frac{P_{11}}{RR_{TPP}}\right) * 100\ \%$
P release from the sediments (mmol m^{-2} d^{-1})		
Benthic P fluxes (F_{TPO4}) and the potential diffusive P fluxes were determined as descried in the methods		
(11)	P release from POP degradation according to Redfield (C/P = 106)	$F_{P(Red)} = F_{DIC}/106$
(12)	True P release from POP	$F_{P(POP)} = F_{DIC} / \left(\frac{POC}{POP}\right)$
(13)	P release from total particulate phosphorus	$F_{P(TPP)} = F_{DIC} / \left(\frac{POC}{TPP}\right)$
(14)	P release from the dissolution of Fe (oxyhydr)oxides (Fe/P = 10, Slomp et al., 1996)	$F_{P(Fe)} = F_{Fe2+} / \left(\frac{Fe}{P}\right)$
(15)	P deficit to outbalance the P budget	$F_{P(deficit)} = RR_{TPP} + RR_{terr} + F_{P(Fe)} - (F_{TPO4} + F_{Pbur})$

1069

1070

1071 **Table 3**: In situ benthic chamber TPO_4 fluxes in mmol m^{-2} d^{-1} along the 12°S transect. The
1072 numbers are shown as an average calculated from the minimum and maximum flux
1073 determined from two benthic chambers. In the cases where only a single number is displayed,
1074 the benthic flux was determined from only one benthic chamber.

Station		Water depth (m)	F_{TPO4} (mmol $m^{-2}d^{-1}$)
I	**BIGO1_2**	74	1.04 ± 0.31
II	**BIGO1_5**	101	0.35 ± 0.01
III	**BIGO2_4**	128	0.30 ± 0.05
IV	**BIGO1_1**	141	0.23 [a]
V	**BIGO1_4**	195	0.12 [a]
VI	**BIGO2_2**	243	0.44 ± 0.07
VII	**BIGO2_1**	306	0.26 ± 0.04
VIII	**BIGO2_5**	409	-0.07 [a]
IX	**BIGO2_3**	756	0.06 [a]
X	**BIGO1_3**	989	0.02 ± 0.02

1075 [a] only one benthic flux was measured

Table 4: Measured and calculated parameters for the P mass balance along the 12°S transect. The numbers in front of key parameters correspond to equations in Table 2.

	Transect section I				Transect section II						Phosphorite formation	
12°S	**Station I**		**Station III**		**Station IV**		**Station V**		**Station VI**		**Station VIII**	
	74 m		**128 m**		**141 m**		**195 m**		**244 m**		**407 m**	
Benthic chamber TPO_4 flux (F_{TPO4})* mmol m^{-2} d^{-1}	1.04	± 0.31	0.3	± 0.05	0.23	-	0.12	-	0.44	± 0.07	-0.07	-
Potential (diffusive) TPO_4 flux (pot. F_{TPO4}) mmol m^{-2} d^{-1}	1.07	± 0.23	2.0	-	0.5	-	1.6		1.5	-		
Relative abundance of Marithioploca-related bacteria* copies g^{-1} (0-5 cm sediment depth)	4159				1687		3072				190	
Benthic chamber DIC flux (F_{DIC})** mmol m^{-2} d^{-1}	65.9	± 21	20.4	± 7	8	± 0.4	3.2	± 1	4.7	± 1	2.2	± 0.3
POC rain rate (RR_{POC})** mmol m^{-2} d^{-1}	79.5	± 33	28.2	± 12	10.5	± 3	12.5	± 6	10.6	± 4	2.7	± 1
Sediment accumulation rate (ω_{acc})** cm yr^{-1}	0.45	± 0.09	0.2	± 0.04	0.04	± 0.008	0.1	± 0.02	0.07	± 0.014	0.01	± 0.002
Mass accumulation rate (MAR)** g m^{-2} yr^{-1}	1800	± 360	600	± 120	128	± 26	320	± 64	182	± 37	44	± 9
Ratios for particulate matter from the water column (2 to 5 m above the sea floor):												
POC/TPP*	76	± 4	68	± 9	94	± 10	132	± 36	62	± 9	96	± 9
POC/PIP*	197	± 17	125	± 34	291	± 79	385	± 7	217	± 34	209	±34
POC/POP*	126	± 17	149	± 29	142	± 3	214	± 87	87	± 29	178	±29
(4) TPP rain rate (RR_{TPP})	1.00	± 0.31	0.40	± 0.09	0.11	±0.02	0.09	± 0.02	0.17	± 0.02	0.03	± 0.01

mmol m^{-2} d^{-1}												
(5) PIP rain rate (RR_{PIP}) mmol m^{-2} d^{-1}	0.39	± 0.14	0.22	± 0.04	0.04	± 0	0.03	± 0.02	0.05	± 0.01	0.01	± 0.01
(6) POP rain rate (RR_{POP}) mmol m^{-2} d^{-1}	0.61	± 0.18	0.18	± 0.05	0.07	±0.02	0.06	± 0.01	0.12	± 0.01	0.01	± 0.01
(7) Terrigenous P input (RR_{Pterr})	0.10	-	0.02	-	0.01	-	0.02	-	0.01	-	0.00	-
(8) Burial flux (F_{Pbur}) in 11 cm sediment depth mmol m^{-2} d^{-1}	0.23	-	0.09	-	0.02	-	0.08	-	0.04	-	0.13	-
Avg. Al conc. (0-1 cm sediment)(Al_{0-1})* mmol g^{-1}	0.99	-	0.70	-	1.10	-	0.97	-	0.72	-	0.66	-
Avg. P conc. (0-11 cm sediment (P_{11})* mmol g^{-1}	0.05	-	0.05	-	0.07	-	0.09	-	0.08	-	1.05	-
(10) P burial efficiency (PBE) at11 cm sediment depth %	26	± 8	23	± 4	23	± 5	92	± 20	23	± 2	490	± 100
(11) P release from POP degradation according to Redfield ($F_{P(Red)}$) mmol m^{-2} d^{-1}	0.62	± 0.2	0.19	± 0.06	0.08	± 0.01	0.03	± 0.01	0.04	± 0.02	0.02	± 0
(12) P release from POP degradation ($F_{P(POP)}$) mmol m^{-2} d^{-1}	0.52	± 0.16	0.14	± 0.05	0.06	± 0.01	0.02	± 0.01	0.05	± 0.02	0.01	± 0
(13) P release from TPP degradation ($F_{P(TPP)}$) mmol m^{-2} d^{-1}	0.87	± 0.17	0.3	± 0.1	0.09	± 0.01	0.02	± 0.01	0.08	± 0.02	0.02	± 0.01
Benthic diffusive TPO_4 flux (potential P flux)*	1.08	± 0.23	2.0	-	0.5	-	1.6	-	1.5	-	-	-
Diffusive Fe^{2+} flux (F_{Fe2+})*	0.04	± 0.02	0.01		0.02		0.0		0.03		0.0	
(14) P release from Fe	0.004	± 0.002	0.001		0.002		0.0		0.003		0.0	

(oxyhydr)oxides ($F_{P(Fe)}$) mmol m^{-2} d^{-1}												
(15) P deficit to outbalance the P budget ($F_{P(deficit)}$) mmol m^{-2} d^{-1}	-	-		0.12	-	0.09	-	0.3	-		-	

1078 * this study

1079 **published data from Dale et al. (2015)

Figure captions

Figure 1: Study area, sampling stations and O_2 concentration in µM along the 12°S transect.

Figure 2A: Concentration profiles of TPP, PIP, POP and POC of the water-column particles and the surface sediments along the 12°S transect. Water-column particle concentrations (upper panel) are given in µmol L^{-1} and surface sediment concentrations (lower panel) are shown in µmol mg^{-1}. Note that the water-column particle concentrations shown for station VI (244 m) at 10 m water depth are ~ 5 times higher than at the other stations.

Figure 2B: Ratios of POC to TPP, PIP and POP (POC/xP) along the 12°S depth transect of water-column particles and surface sediments (0 – 5.5 cm depth) of station I to VIII (74 to 407 m).

Figure 3: Average distribution of POP and PIP (%) per station in the water-column particles and in the top 5.5 cm of the sediments.

Figure 4A: Measured benthic TPO_4 fluxes (mmol m^{-2} d^{-1}) at 12°S. The black line shows the theoretical TPO_4 flux generated from organic matter degradation with a Redfield POC/POP ratio of 106.

Figure 4B: Potential TPO_4 fluxes (mmol m^{-2} d^{-1}) calculated from porewater profiles compared to the measured benthic TPO_4 fluxes (mmol m^{-2} d^{-1}) at stations I to VIII (74 to 407 m). The black line with triangles depicts the TPO_4 flux that could be generated during degradation of total particulate phosphorus.

Figure 4C: P percentages of the different P sources and the missing P that is needed to maintain the measured TPO_4 release rates and P burial fluxes for stations IV, V and VI (141, 195 and 244 m) of transect section II. The missing P is assumed to be supplied by sulfide-oxidizing Marithioploca-related bacteria (see Discussion).

Figure 5: Mass balance calculations and measured benthic TPO_4 fluxes for stations I to VIII (74 to 407 m). All fluxes are in mmol m^{-2} d^{-1}

Figure 5A: POP rain rates, TPO_4 fluxes and P burial rates only. The number in percent denotes missing P needed to sustain the benthic TPO_4 fluxes.

Figure 5B: Mass balance calculations including the POP and PIP rain rates, the terrigenous P input, P release from the reductive dissolution of Fe (oxyhydr)oxides and the benthic TPO_4 fluxes into the bottom waters as well as the P burial rates.

Figure 6: Measured TPO_4 fluxes versus relative abundance of Marithioploca in cells g^{-1} in the upper 5 cm of the sediment. Highest abundance and TPO_4 flux was found at station I. The other data points are for the stations IV, VI and VIII (with decreasing abundance and TPO_4 flux).

Figure 7: Comparison of pore water PO_4^{3-} concentrations before (blue) and after the freeze/thaw experiments (red) in µmol L^{-1}.

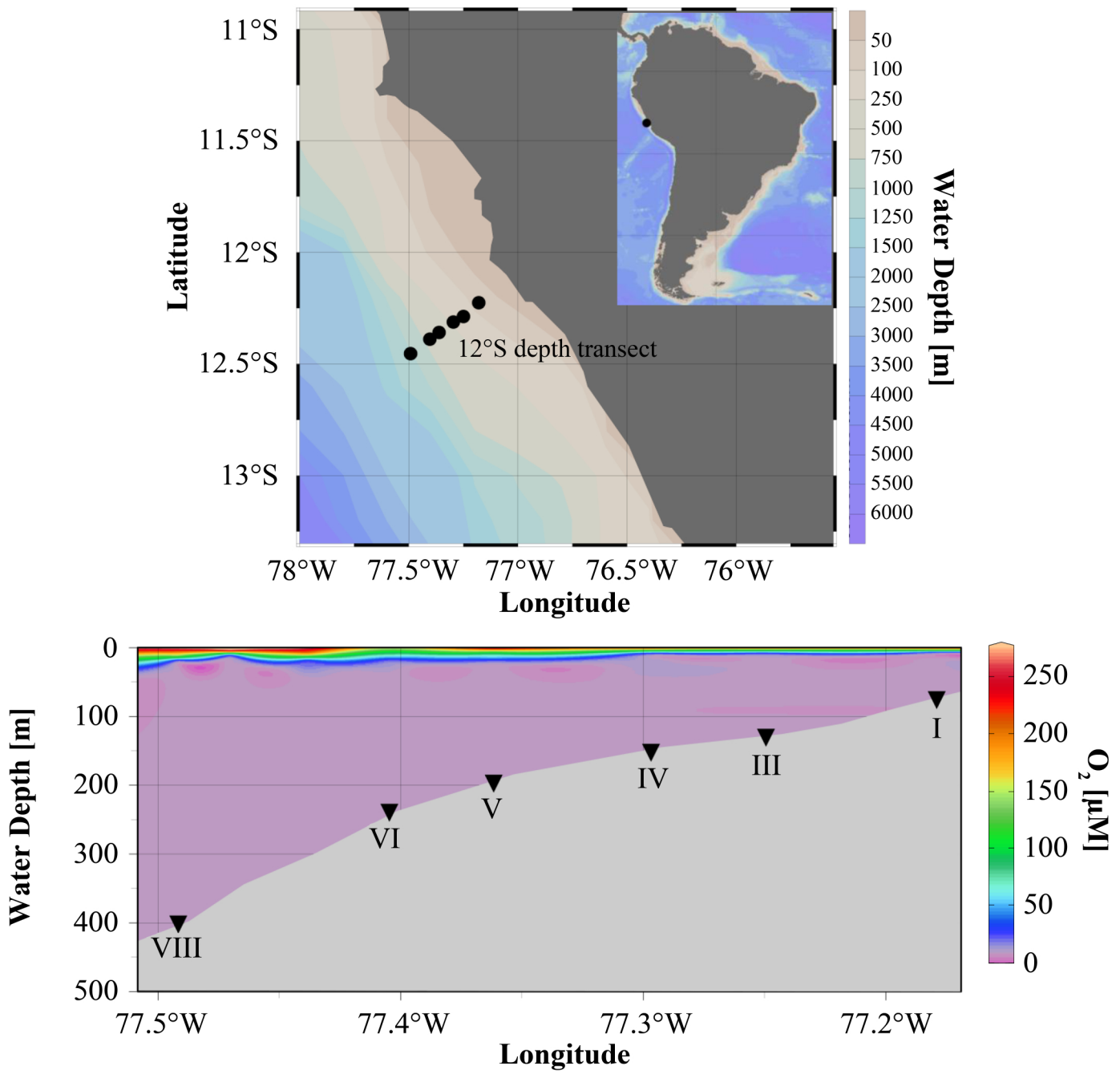
11°S
11.5°S
12°S
12.5°S
13°S
Latitude
12°S depth transect
78°W
77.5°W
77°W
76.5°W
76°W
Longitude
50
100
250
500
750
1000
1250
1500
2000
2500
3000
3500
4000
4500
5000
5500
6000
Water Depth [m]
0
100
200
300
400
500
Water Depth [m]
VIII
VI
V
IV
III
I
77.5°W
77.4°W
77.3°W
77.2°W
Longitude
250
200
150
100
50
0
O2 [µM]

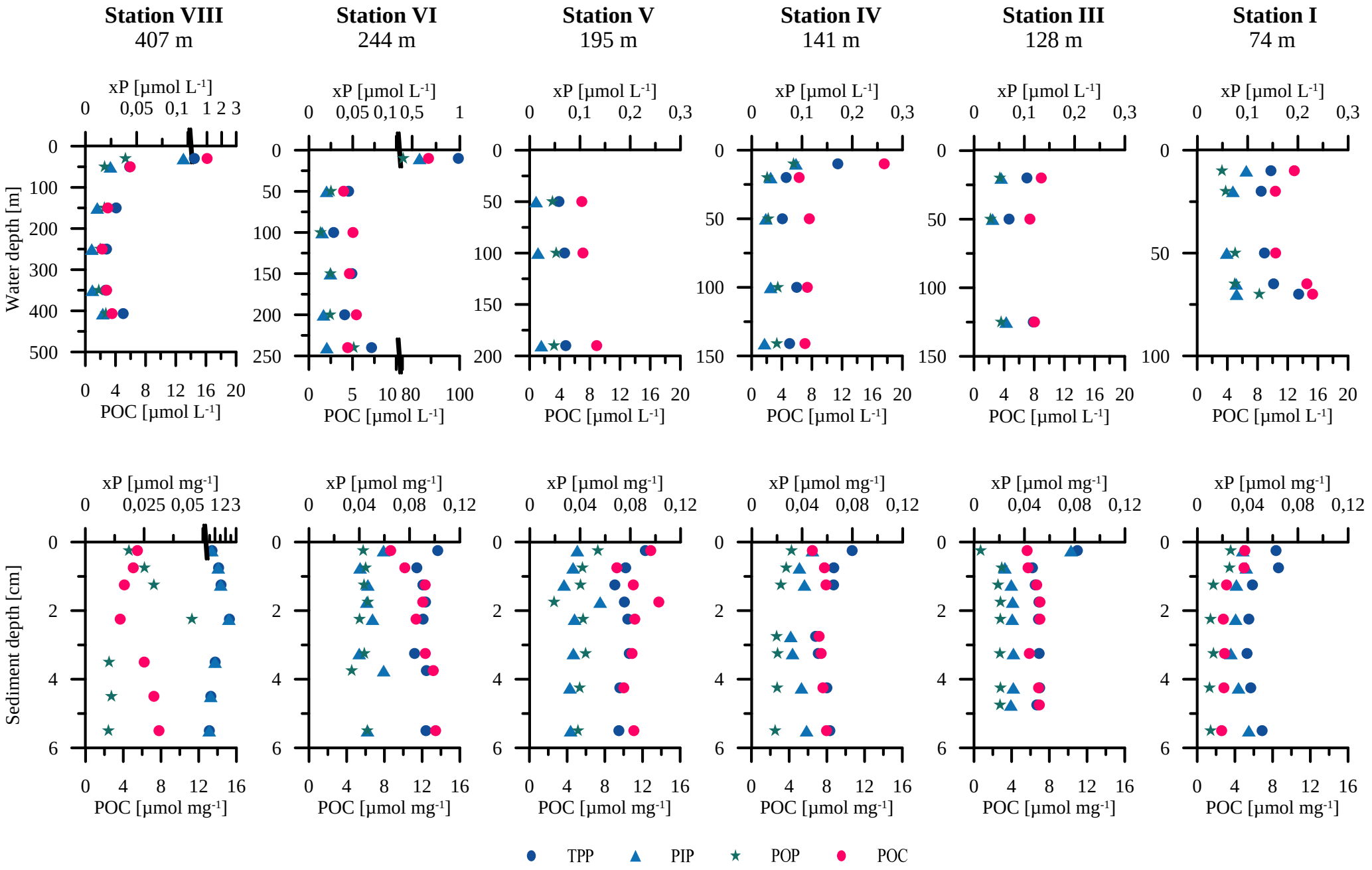
Station VIII
407 m
Station VI
244 m
Station V
195 m
Station IV
141 m
Station III
128 m
Station I
74 m
xP [µmol L-1]
Water depth [m]
POC [µmol L-1]
xP [µmol mg-1]
Sediment depth [cm]
POC [µmol mg-1]
TPP
PIP
POP
POC

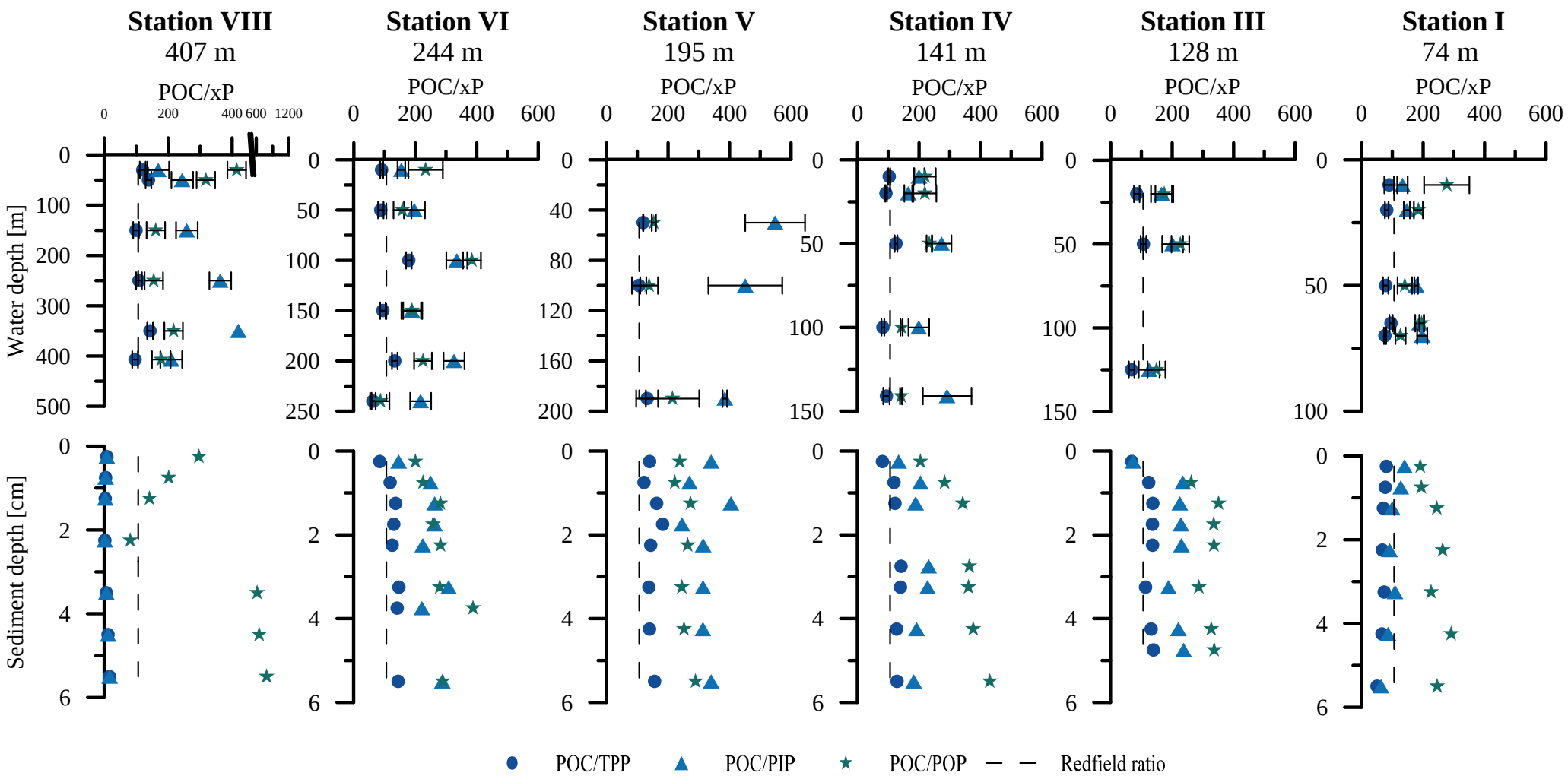
Station VIII
407 m
Station VI
244 m
Station V
195 m
Station IV
141 m
Station III
128 m
Station I
74 m
POC/xP
Water depth [m]
Sediment depth [cm]
POC/TPP
POC/PIP
POC/POP
Redfield ratio

Water column particles

%

100
80
60
40
20
0

POP

PIP

Sediments

%

100
80
60
40
20
0

POP

PIP

VIII VI V IV III I

Station

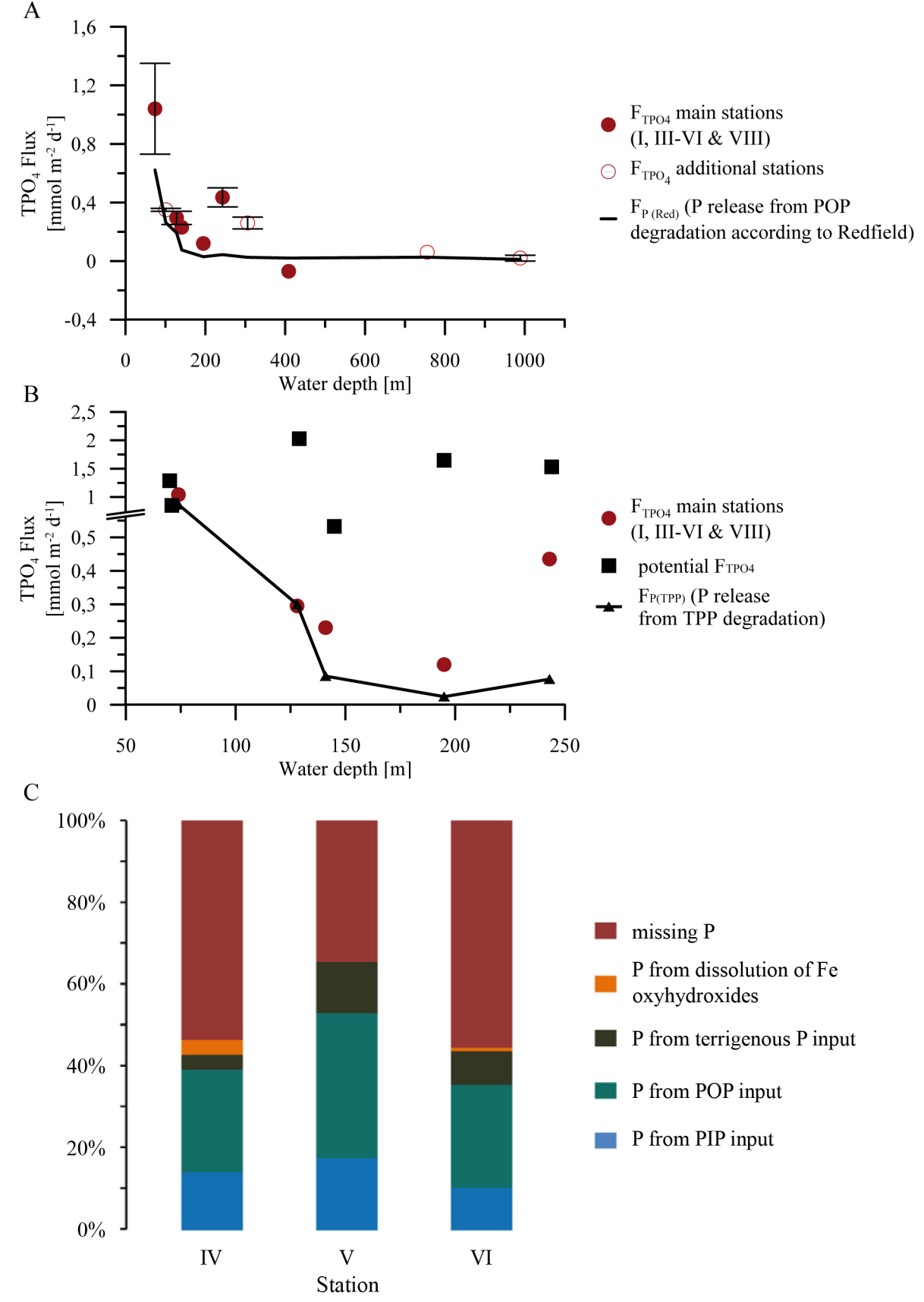
A
1,6
1,2
0,8
0,4
0
-0,4
TPO4 Flux
[mmol m-2 d-1]
0
200
400
600
800
1000
Water depth [m]
FTPO4 main stations
(I, III-VI & VIII)
FTPO4 additional stations
FP (Red) (P release from POP
degradation according to Redfield)
B
2,5
2
1,5
1
0,5
0,4
0,3
0,2
0,1
0
TPO4 Flux
[mmol m-2 d-1]
50
100
150
200
250
Water depth [m]
FTPO4 main stations
(I, III-VI & VIII)
potential FTPO4
FP(TPP) (P release
from TPP degradation)
C
100%
80%
60%
40%
20%
0%
IV
V
VI
Station
missing P
P from dissolution of Fe
oxyhydroxides
P from terrigenous P input
P from POP input
P from PIP input

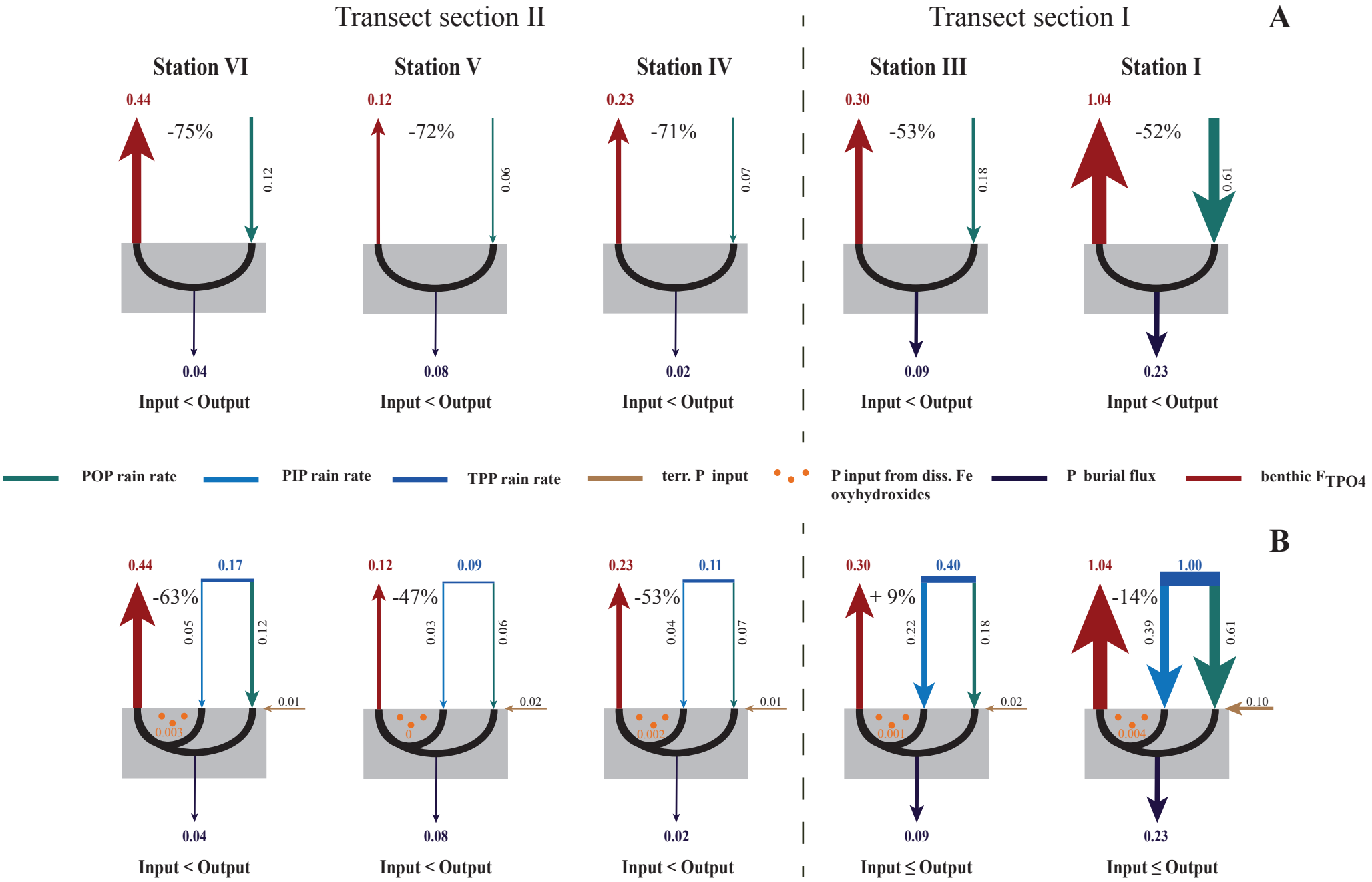
Transect section II
Transect section I
A
Station VI
Station V
Station IV
Station III
Station I
0.44
-75%
0.12
0.04
Input < Output
0.12
-72%
0.06
0.08
Input < Output
0.23
-71%
0.07
0.02
Input < Output
0.30
-53%
0.18
0.09
Input < Output
1.04
-52%
0.61
0.23
Input < Output
POP rain rate
PIP rain rate
TPP rain rate
terr. P input
P input from diss. Fe oxyhydroxides
P burial flux
benthic F$_{TPO4}$
B
0.44
0.17
-63%
0.05
0.12
0.01
0.003
0.04
Input < Output
0.12
0.09
-47%
0.03
0.06
0.02
0
0.08
Input < Output
0.23
0.11
-53%
0.04
0.07
0.01
0.002
0.02
Input < Output
0.30
0.40
+ 9%
0.22
0.18
0.02
0.001
0.09
Input ≤ Output
1.04
1.00
-14%
0.39
0.61
0.10
0.004
0.23
Input ≤ Output

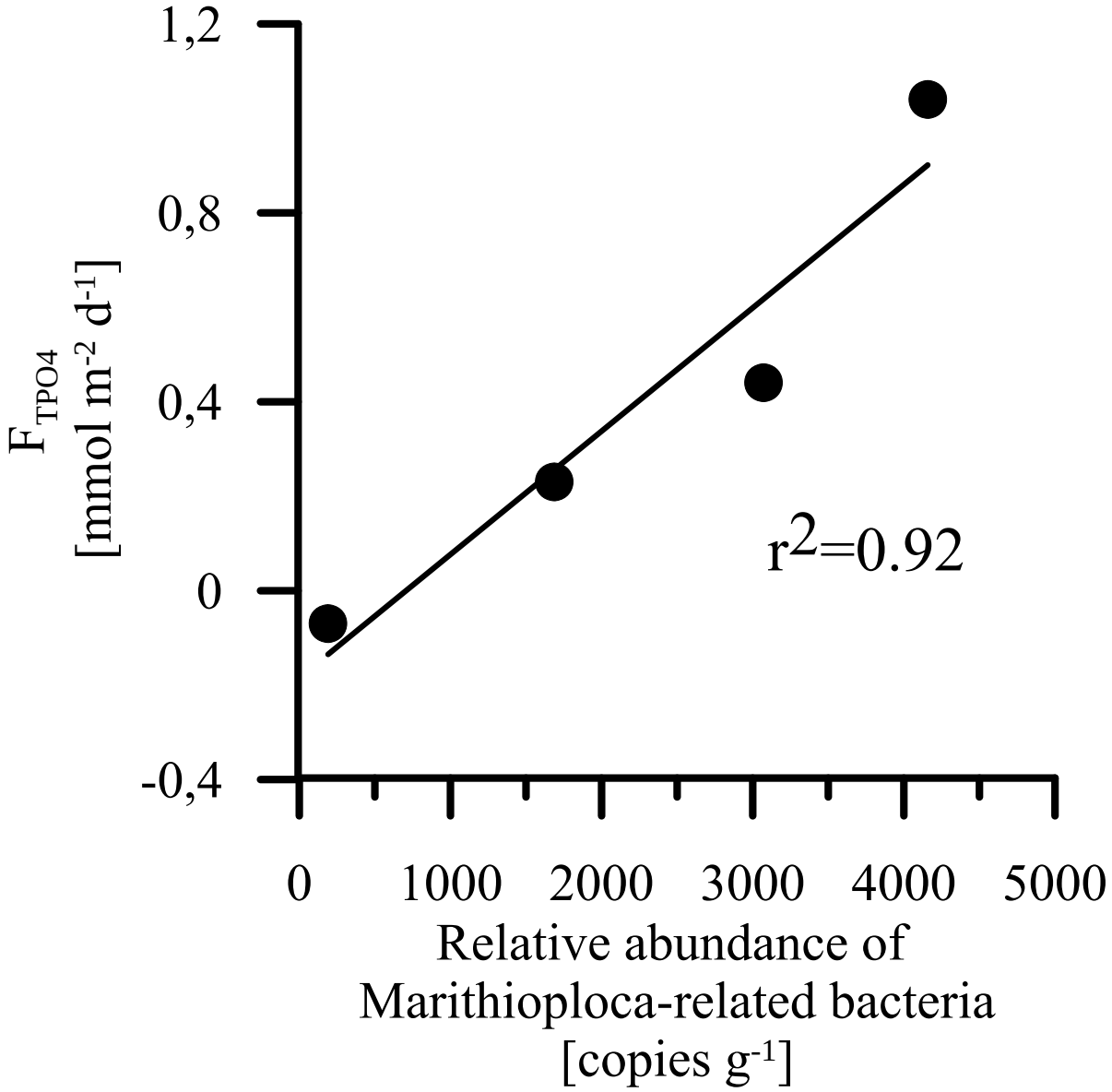
1,2
0,8
0,4
0
-0,4
F_{TPO4} [mmol m^{-2} d^{-1}]
r^2=0.92
0
1000
2000
3000
4000
5000
Relative abundance of Marithioploca-related bacteria [copies g^{-1}]

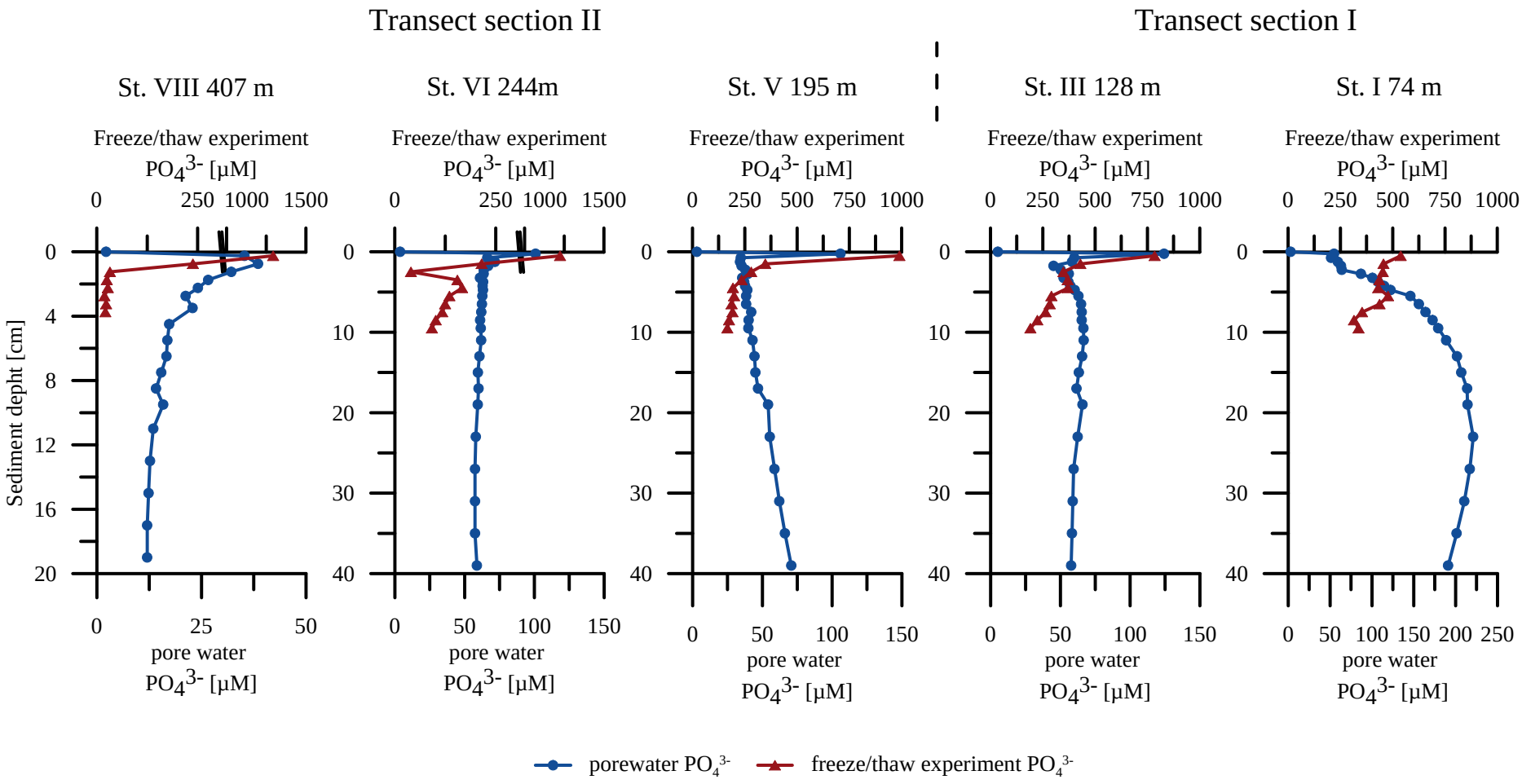
Transect section II
Transect section I
St. VIII 407 m
St. VI 244m
St. V 195 m
St. III 128 m
St. I 74 m
Freeze/thaw experiment
PO4 3- [µM]
Sediment depht [cm]
pore water
PO4 3- [µM]
porewater PO4 3-
freeze/thaw experiment PO4 3-